Journal of Asian Earth Sciences 98 (2015) 247–260

Contents lists available at ScienceDirect

Journal of Asian Earth Sciences

journal homepage: www.elsevier.com/locate/jseaes

Zircon U–Pb geochronological, geochemical, and Sr–Nd isotope data for Early Cretaceous mafic dykes in the Tancheng–Lujiang Fault area of the Shandong Province, China: Constraints on the timing of magmatism and magma genesis

Shen Liu [a,*], Caixia Feng [a], Ruizhong Hu [b], Mingguo Zhai [a], Shan Gao [c], Shaocong Lai [a], Jun Yan [b], Ian M. Coulson [d], Haibo Zou [e]

[a] State Key Laboratory of Continental Dynamics and Department of Geology, Northwest University, Xi'an 710069, China
[b] State Key Laboratory of Ore Deposit Geochemistry, Institute of Geochemistry, Chinese Academy of Sciences, Guiyang 550002, China
[c] State Key Laboratory of Geological Processes and Mineral Resources, China University of Geosciences, Wuhan 430074, China
[d] Solid Earth Studies Laboratory, Department of Geology, University of Regina, Regina, Saskatchewan S4S 0A2, Canada
[e] Faculty of Earth Sciences, China University of Geosciences, Wuhan 430074, China

ARTICLE INFO

Article history:
Received 20 August 2014
Received in revised form 28 October 2014
Accepted 11 November 2014
Available online 29 November 2014

Keywords:
Age
Origin
Hybridization
Tan–Lu Fault
NCC
Yangtze Craton

ABSTRACT

The timing and source of magmatism that formed Early Cretaceous dolerite dykes in the Tancheng–Lujiang (Tan–Lu) Fault area of the southeastern North China Craton was determined using geochronological, geochemical, and whole-rock Sr–Nd isotopic data. Laser ablation–inductively coupled plasma–mass (LA–ICP–MS) spectrometry U–Pb analysis of zircon yielded consistent ages of 129.6 ± 0.7, 126.8 ± 0.7, 125.5 ± 0.7, 124.9 ± 0.9, 126.4 ± 0.7, and 125.5 ± 0.7 Ma for six samples of the mafic dykes within the NCC. The $K_2O + Na_2O$ concentrations (5.02–5.21 wt.%) of the dykes indicate they are alkaline and these dykes have K_2O concentrations (2.35–2.48 wt.%) that indicate they are shoshonitic. These dolerites are also characterized by high and wide ranging $(La/Yb)_N$ (14.5–36.0), have slightly negative Eu anomalies (δEu = 0.70–0.91) and positive Ba, U, K, and Pb anomalies, and are depleted in the high field strength elements (Nb, Ta, P, and Ti). In addition, these mafic dykes are characterized by high radiogenic Sr $[(^{87}Sr/^{86}Sr)_i = 0.7099–0.7100]$ and negative $\varepsilon_{Nd}(t)$ values (−14.4 to −13.7). These data suggest that the magmas that formed the dykes were derived through the partial melting (12.0–15.0%) of an enriched region of the mantle that was hybridized during interaction with subducted sedimentary rocks from the Yangtze Craton. The parental magmas then fractionated olivine and Fe–Ti oxides during ascent and underwent negligible crustal contamination during magma emplacement. These mafic magmas were finally emplaced as dyke swarms associated with lithospheric extension.

0. Introduction

China hosts three cratons, namely the North China Craton (NCC), the Yangtze Craton, and the Tarim Craton. This study focuses on the NCC, which formed during the Precambrian (2.5 Ga; Wu et al., 1998; Zhai and Bian, 2000), contains ancient continental crust (Wang et al., 1998, 2007; Zheng et al., 2004; Gao et al., 2005; Wan et al., 2005; Diwu et al., 2008; Chen et al., 2009; Zhang et al., 2009), and is cross-cut by swarms of Precambrian (2.5–0.8 Ga; Zhai and Bian, 2000; Peng et al., 2005, 2007, 2008, 2010, 2011a,b; Hou et al., 2006; Peng, 2010; Hou, 2012) and Mesozoic (169.5–83.2 Ma; Liu et al., 2004, 2005, 2006, 2008a,b, 2009a, 2012, 2013a,b) mafic dykes. It is generally accepted that intense destruction and thinning of the lithosphere within the NCC occurred during the Mesozoic.

Belts of lithosphere extension are currently of great interest in terms of geodynamic research, and this type of extensional tectonics is commonly associated with the intrusion of mafic dykes (e.g., lamprophyre, diorite, and porphyritic dolerite dykes), which can provide useful information on the processes that operated during extension, the sourcing of the magmas, and the geodynamic evolution of an area. However, research in the NCC has generally focused on Precambrian (e.g., more than 100 studies in Hebei, Shanxi, and Shandong provinces) and Mesozoic (more than 700 studies in Jilin, Liaoning, Shanxi, Hebei, Shandong, Gansu, Shaanxi, and Henan

* Corresponding author. Tel.: +86 29 88300225.
E-mail address: liushen@vip.gyig.ac.cn (S. Liu).

http://dx.doi.org/10.1016/j.jseaes.2014.11.001
1367-9120/

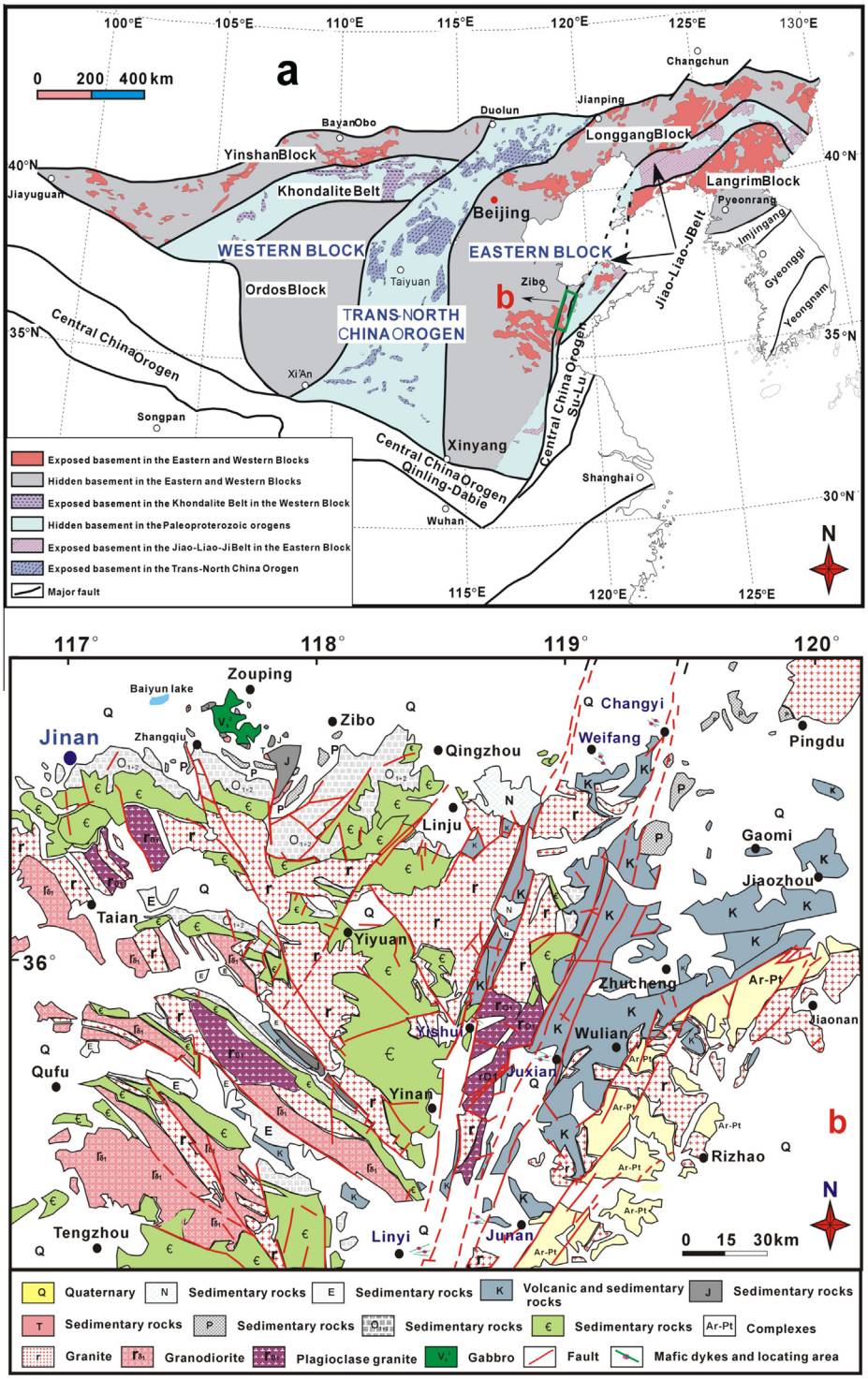

Fig. 1. (a) Location of the study area within the NCC. (b) Geological map of the study area, showing the regions of samples obtained during this study.

Provinces, and Inner Mongolia Autonomous Region) dykes within stable tectonic blocks (e.g., in orogenic zones and intraplate tectonic settings; Li et al., 1997; Zhai and Bian, 2000; Liu et al., 2004, 2005, 2006, 2008a,b,c, 2009a, 2012, 2013a,b,c,d,e; Peng et al., 2005, 2007, 2008, 2010, 2011a,b; Hou et al., 2006; Peng, 2010; Hou, 2012), with comparatively few studies focusing on the mafic dykes within fault zones. The Tan–Lu Fault is a very important fault zone within China. At present, the formation period for the Tan–Lu Fault is controversial (Xu, 1993; Yin and Nie, 1993; Li, 1994; Tang et al., 1995; Wan and Zhu, 1996; Zhang, 1997; Wang et al., 2000; Xiao et al., 2000; Qian et al., 2001; Qiao et al., 2001; Qiao and Zhang, 2002; Luo et al., 2005). However, it is accepted that the Tu–Lu Fault likely formed during the Neoarchaean and was reactivated during both the Neoproterozoic and the Mesozoic. Furthermore, movement on this Fault zone has also been noted for the Palaeozoic. In addition, the Fault formed as a result of lithospheric extension between the late Mesozoic and the Palaeogene (Xu and Ma, 1992; Zhu et al., 2001, 2005; Liu

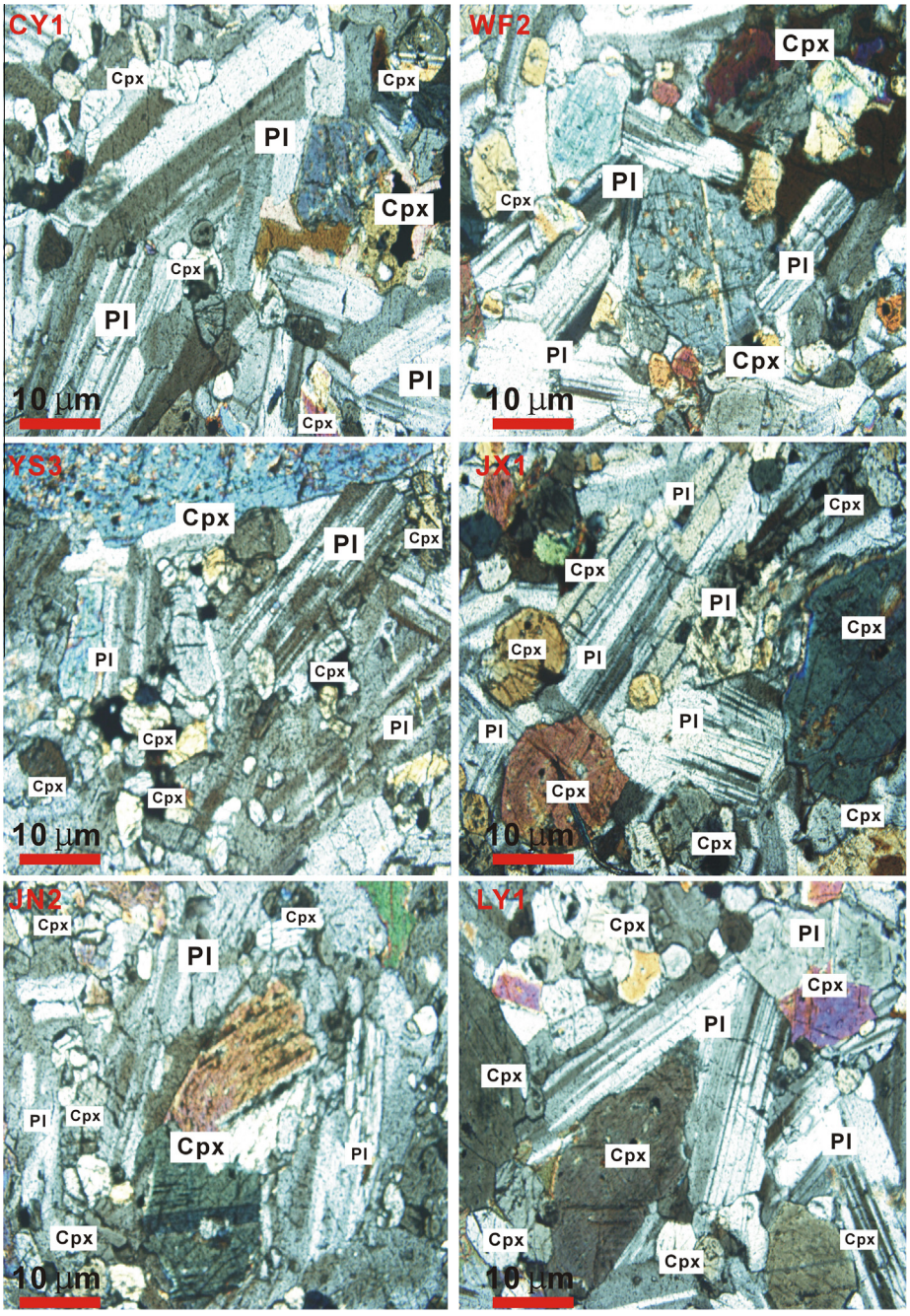

Fig. 2. Representative photomicrographs of the mafic dykes from the southeastern NCC, China. All of these samples have doleritic textures and hence are termed dolerite dykes. Py = pyroxene, Pl = plagioclase.

et al., 2002; Wang et al., 2006; Xie et al., 2007), and is considered to be a classic model of lithospheric extension. Systematic investigation of the extension that occurred during the formation of the Tan–Lu Fault can not only provide valuable information on the timing of and processes involved in extension in this area but can also enhance our knowledge of geodynamic systems. The dynamic mechanism and setting of the extension that formed the Tan–Lu Fault has not as yet been the focus of systematic research, primarily because of the limited availability of data from the surrounding basins. Mesozoic magmatism was widespread throughout the Tan–Lu Fault zone, and needs to be incorporated into any model for the dynamic setting of this Fault. However, previous research in this area has focused only on intermediate and felsic volcanic rocks (Niu et al., 2001, 2002, 2005, 2007; Zhu et al., 2001, 2005; Xie et al., 2008, 2009; Zhu et al., 2010), monzonites, and granites (Niu et al., 2002, 2008); units that are present along only a small part of the Fault zone, meaning that these rocks can provide only limited information on the extensional regime that controlled the development of the Tan–Lu Fault.

This lack of data indicates that a more detailed geochronological, geochemical, and isotopic study of a variety of Mesozoic mafic dykes from the Tan–Lu Fault is required to further refine the extensional processes and geotectonic background that operated during the formation of this Fault zone. Here, we present the results of new zircon U–Pb dating using LA–ICP–MS, as well as petrological, whole-rock geochemical, and Sr–Nd isotopic data for representa-

Table 1
LA–ICP–MS U–Pb isotope data for zircons from the mafic dykes within the Tan–Lu Fault zone.

CY01						Isotopic ratios						Age (Ma)					
Spot	Th	U	Pb	Th/U	$^{238}U/^{232}Th$	$^{207}Pb/^{206}Pb$	1σ	$^{207}Pb/^{235}U$	1σ	$^{206}Pb/^{238}U$	1σ	$^{207}Pb/^{206}Pb$	1σ	$^{207}Pb/^{235}U$	1σ	$^{206}Pb/^{238}U$	1σ
1	684	1167	59	0.59	1.69	0.0522	0.0022	0.1345	0.0046	0.0202	0.0002	296	82	139	6	129	1
2	239	489	131	0.49	2.05	0.0519	0.0019	0.1363	0.0052	0.0203	0.0004	281	74	139	6	130	2
3	327	461	45	0.71	1.41	0.0525	0.0024	0.1354	0.0035	0.0197	0.0001	307	84	139	6	130	1
4	1245	947	169	1.31	0.78	0.0526	0.0025	0.1406	0.0028	0.0203	0.0003	312	79	139	6	131	2
5	1085	541	137	2.01	0.54	0.0525	0.0024	0.1345	0.0046	0.0196	0.0005	307	67	139	6	131	3
6	729	499	54.6	1.46	0.67	0.0524	0.0023	0.1373	0.0045	0.0204	0.0002	302	81	139	6	130	1
7	488	614	55.7	0.79	0.65	0.0520	0.0025	0.1403	0.0041	0.0203	0.0003	284	67	140	6	130	2
8	606	517	43.3	1.17	0.74	0.0529	0.0021	0.1353	0.0025	0.0198	0.0002	322	93	140	6	130	1
9	1956	1523	161	1.28	0.76	0.0533	0.0044	0.1354	0.0024	0.0201	0.0002	342	188	141	11	129	1
10	594	573	50.0	1.04	0.94	0.0461	0.0044	0.1402	0.0036	0.0203	0.0004		199	126	11	129	2
11	5165	4034	495	1.28	0.98	0.0463	0.0040	0.1366	0.0043	0.0202	0.0002	11	189	128	10	129	1
WF02																	
1	538	1145	104	0.47	0.75	0.0461	0.0019	0.1293	0.0079	0.0197	0.0003		88	120	4	126	2
2	1115	2299	135	0.49	0.73	0.0466	0.0031	0.1296	0.0066	0.0199	0.0002	30	145	122	8	127	1
3	2134	1512	148	1.41	0.71	0.0530	0.0021	0.1292	0.0083	0.0198	0.0002	329	85	139	6	126	1
4	611	878.3	444	0.70	0.75	0.0535	0.0046	0.1318	0.0114	0.0199	0.0003	349	197	139	11	127	2
5	1250	1598	207	0.78	0.76	0.0573	0.0061	0.1313	0.0104	0.0198	0.0004	502	243	147	14	126	2
6	1041	3486	158	0.30	0.78	0.0560	0.0041	0.1307	0.0101	0.0199	0.0002	452	169	145	10	127	1
7	3909	3004	557	1.30	0.92	0.0481	0.0058	0.1327	0.0109	0.0202	0.0004	105	249	127	14	128	3
8	10,216	4564	516	2.24	0.91	0.0522	0.0045	0.1323	0.0114	0.0198	0.0002	292	196	135	11	126	1
9	606	947	80.5	0.64	0.78	0.0507	0.0063	0.1324	0.0101	0.0200	0.0004	227	275	133	15	127	2
10	5158	4021	483	1.28	0.96	0.0473	0.0037	0.1311	0.0112	0.0201	0.0002	66	176	125	9	128	1
11	608	954	85.3	0.64	0.79	0.0527	0.0068	0.1334	0.0109	0.0199	0.0003	315	292	137	16	127	2
12	612	963	90.6	0.64	0.77	0.0507	0.0047	0.1316	0.0115	0.0200	0.0002	228	214	133	12	127	1
13	5172	4046	511	1.28	0.97	0.0472	0.0040	0.1307	0.0092	0.0201	0.0003	59	188	125	10	128	2
YS01																	
1	408	581	31.7	0.70	0.63	0.0519	0.0024	0.1353	0.0067	0.0196	0.0003	281	80	134	6	125	2
2	227	144	15.2	1.58	0.63	0.0518	0.0023	0.1352	0.0065	0.0197	0.0003	277	82	134	6	126	2
3	1023	895	93.9	1.14	0.63	0.0516	0.0023	0.1354	0.0068	0.0195	0.0004	268	76	134	6	124	2
4	642	466	41.2	1.38	1.40	0.0772	0.0028	0.1356	0.0083	0.0198	0.0002	1126	63	198	7	126	1
5	637	906	66.5	0.70	1.40	0.0475	0.0034	0.1361	0.0092	0.0195	0.0002	76	161	122	8	125	1
6	48.8	74.2	27.2	0.66	1.40	0.0461	0.0027	0.1352	0.0073	0.0197	0.0002		128	120	7	126	1
7	764	513	52.8	1.49	1.40	0.0464	0.0029	0.1354	0.0077	0.0196	0.0002	20	138	120	7	125	1
8	895	974	72.8	0.92	1.40	0.0480	0.0032	0.1356	0.0085	0.0198	0.0002	97	148	125	8	126	1
9	428	342	30.1	1.25	1.40	0.0465	0.0029	0.1356	0.0076	0.0196	0.0002	24	135	120	7	125	1
10	628	477	45.1	1.32	0.78	0.0481	0.0016	0.1352	0.0043	0.0196	0.0002	104	55	129	4	125	1
11	871	677	59.4	1.29	0.78	0.0483	0.0017	0.1354	0.0044	0.0197	0.0002	114	61	129	4	126	1
12	286	453	40.8	0.63	0.78	0.0479	0.0018	0.1361	0.0045	0.0198	0.0004	94	41	130	4	126	3
JX01																	
1	776	919	329	0.84	0.85	0.0587	0.0096	0.1319	0.0061	0.0197	0.0002	554	367	150	23	126	1
2	183	130	17.5	1.41	0.85	0.0557	0.0111	0.1318	0.0056	0.0194	0.0003	441	410	141	26	124	2
3	223	134	17.2	1.66	0.85	0.0541	0.0103	0.1317	0.0057	0.0197	0.0004	375	388	139	25	126	2
4	279	180	19.1	1.55	0.85	0.0562	0.0094	0.1315	0.0052	0.0195	0.0002	460	360	143	22	125	1
5	169	138	184	1.22	0.57	0.0524	0.0023	0.1316	0.0062	0.0194	0.0003	303	71	134	6	124	2
6	196	415	37.1	0.47	0.57	0.0522	0.0023	0.1315	0.0061	0.0195	0.0003	294	67	134	5	124	2
7	665	315	42.8	2.11	0.57	0.0523	0.0024	0.1318	0.0063	0.0197	0.0003	299	78	135	6	126	2
8	87.4	127	40.4	0.69	0.58	0.0528	0.0026	0.1319	0.0066	0.0198	0.0003	320	78	135	6	126	2
9	235	138	17.6	1.70	0.85	0.0526	0.0089	0.1317	0.0058	0.0195	0.0003	312	343	135	21	125	2
10	283	186	20.3	1.52	0.85	0.0542	0.0090	0.1315	0.0064	0.0195	0.0002	380	351	138	21	124	1
11	174	144	192	1.21	0.57	0.0523	0.0022	0.1315	0.0061	0.0195	0.0003	299	70	134	5	124	2
12	218	426	39.5	0.51	0.57	0.0524	0.0023	0.1314	0.0062	0.0194	0.0003	303	68	134	6	124	2

JN01																		
1	988	1561	141	0.63	1.69	0.0465	0.0029	0.1295	0.0065	0.0198	0.0003	24	79	124	6	126	2	
2	1943	1523	155	1.28	2.05	0.5320	0.0022	0.1293	0.0082	0.0197	0.0003	4332	75	123	7	126	2	
3	616	863	436	0.71	1.41	0.5360	0.0045	0.1316	0.0112	0.0198	0.0002	4343	115	126	10	126	1	
4	1242	1462	212	0.85	0.78	0.0572	0.0058	0.1312	0.0103	0.0197	0.0003	499	148	125	9	126	2	
5	984	1612	163	0.61	0.75	0.0561	0.0043	0.1308	0.0102	0.0198	0.0002	456	157	125	9	126	1	
6	3827	3015	566	1.27	0.67	0.0482	0.0056	0.1326	0.0108	0.0199	0.0003	109	153	126	10	127	2	
7	1481	2013	521	0.74	1.27	0.0523	0.0046	0.1322	0.0113	0.0196	0.0004	299	156	126	10	125	3	
8	595	925	88.6	0.64	2.11	0.0506	0.0062	0.1323	0.0101	0.0202	0.0003	223	146	126	9	129	2	
9	5069	4035	497	1.26	0.84	0.0471	0.0036	0.1313	0.0113	0.0203	0.0003	54	162	125	10	130	2	
10	569	865	86.9	0.66	2.06	0.0525	0.0066	0.1332	0.0107	0.0198	0.0002	307	165	127	10	126	1	
11	618	946	93.4	0.65	0.71	0.0506	0.0046	0.1315	0.0113	0.0199	0.0003	223	166	125	10	127	2	
12	5076	4052	516	1.25	0.76	0.0473	0.0042	0.1306	0.0093	0.0198	0.0004	64	119	125	8	126	3	
LY01																		
1	433	571	32.4	0.76	1.42	0.0518	0.0023	0.1352	0.0066	0.0195	0.0002	277	94	129	6	124	1	
2	236	155	15.5	1.52	0.63	0.0519	0.0023	0.1351	0.0065	0.0196	0.0002	281	92	129	6	125	1	
3	1135	963	94.6	1.18	0.85	0.0517	0.0024	0.1353	0.0067	0.0196	0.0003	272	85	129	6	125	2	
4	639	488	41.7	1.31	0.81	0.0771	0.0026	0.1355	0.0081	0.0197	0.0002	1124	107	129	7	126	1	
5	642	883	67.3	0.73	1.40	0.0476	0.0032	0.1362	0.0093	0.0196	0.0003	79	122	130	8	125	2	
6	66.5	86.4	27.8	0.77	2.88	0.0463	0.0026	0.1353	0.0071	0.0198	0.0002	13	96	129	6	126	1	
7	781	565	53.9	1.38	0.70	0.0462	0.0028	0.1352	0.0075	0.0197	0.0002	8	97	129	7	126	1	
8	924	967	73.8	0.96	1.14	0.0481	0.0031	0.1355	0.0083	0.0198	0.0003	104	108	129	7	126	2	
9	445	351	29.6	1.27	0.78	0.0463	0.0028	0.1356	0.0074	0.0195	0.0002	13	97	129	7	124	1	
10	638	482	47.4	1.32	0.74	0.0482	0.0017	0.1353	0.0041	0.0197	0.0003	109	43	129	4	126	2	
11	887	674	61.5	1.32	0.76	0.0481	0.0018	0.1352	0.0043	0.0198	0.0004	104	39	129	4	126	3	
12	292	445	42.3	0.66	2.25	0.0478	0.0016	0.1362	0.0042	0.0196	0.0002	89	53	130	4	125	1	

tive samples of mafic dykes from the southeastern NCC in Shandong Province, China. These new data allow us to constrain the emplacement ages of these dykes and the origin of the mafic magmatism throughout the Tan–Lu Fault zone.

1. Geological setting and petrography

The NCC is one of the oldest cratonic blocks in the world, underlies the majority of northern China, the southern part of northeast China, Inner Mongolia, Bohai Bay, and the northern part of the Yellow Sea, and covers an area of approximately 1,500,000 km^2 (Zhao, 2014). The NCC is split into the eastern and western NCC along the N–S-trending Palaeoproterozoic (1.85 Ga) Trans-North China Orogen (Zhao et al., 2001, 2005; Wilde et al., 2002; Guo et al., 2005a,b). The Tan–Lu Fault starts under the western Pacific Ocean and extends into eastern China (Zhao, 2014). The Fault trends NNE–SSW and stretches for more than 2400 km from south to north, passing through Huangmei in Hubei Province, Lujiang and Jiasan in Anhui Province, Sihong, Suqian, and Xinyi in Jiangsu Province, Tancheng and Weifang in Shandong Province, the Gulf of Bohai, and northeastern China. The Tan–Lu Fault also cross-cuts the NCC, the Yangtze Craton, and the Xingmeng–Jihei and Dabie–Sulu orogenic belts (Yan et al., 2008). The Fault has been studied for more than 40 years (Xu and Zhu, 1994; Zhu et al., 1995, 2000, 2010; Niu et al., 2008), leading to a generally accepted evolutionary history in which the Tan–Lu Fault underwent strike-slip movement between the Late Jurassic and Early Cretaceous, extensional movement between the Late Cretaceous and Palaeogene, and compression since the Neogene (Xu and Ma, 1992; Zhu et al., 2001, 2005; Wang et al., 2006; Xie et al., 2007; Niu et al., 2008).

The Tan–Lu Fault is also called the Yi–Shu Fault in Shandong Province and hosts more than 150 Mesozoic mafic dykes. The mafic magmatism responsible for these dykes was widely distributed across the Tan–Lu Fault zone and, as such, is critically important to investigating the geodynamics of this Fault. Nevertheless, earlier studies have mainly focused on felsic-intermediate magmatism along the Tan–Lu Fault zone, and the swarms of mafic dykes have, for the most part, been paid little attention (e.g., Liu et al., 2004, 2005, 2006, 2008a,b, 2009a, 2012, 2013a,b). To address these deficiencies, this study focuses on mafic dykes from across the Changyi, Weifang, Yishui, Juxian, Junan, and Linyi regions of central Shandong Province (samples CY1 to CY4, WF1 to WF4, YS1 to YS4, JX1 to JX4, JN1 to JN4, and LY1 to LY4, respectively). The mafic dykes in these areas were intruded into both Proterozoic complexes and early Mesozoic sedimentary rocks (Figs. 1b and 2 in addition to field observations and notes). Individual dykes are vertical, trend NE–SW, NW–SE, and nearly E–W and N–S, commonly 0.6–18 m wide, and are 2.5–15 km long. Representative hand specimens and photomicrographs of the mafic dykes sampled during this study are shown in Fig. 2. The dykes are generally medium-grained dolerites that contain clinopyroxene (2.0–6.0 mm) and plagioclase (2.0–5.5 mm) phenocrysts in a matrix (60–65%) that contains clinopyroxene (0.05–0.06 mm) and plagioclase (0.03–0.05 mm) with minor magnetite (~0.02–0.03 mm) and chlorite (0.03–0.05 mm), and accessory zircon and apatite.

2. Analytical techniques

2.1. Zircon LA–ICP–MS U–Pb dating

Zircon grains were separated from six samples (CY01, WF02, YS01, JX01, JN01, and LY02) using conventional heavy liquid and magnetic techniques at the Langfang Regional Geological Survey, Hebei Province, China. After separation and mounting, zircon internal and external structures were imaged using both transmitted

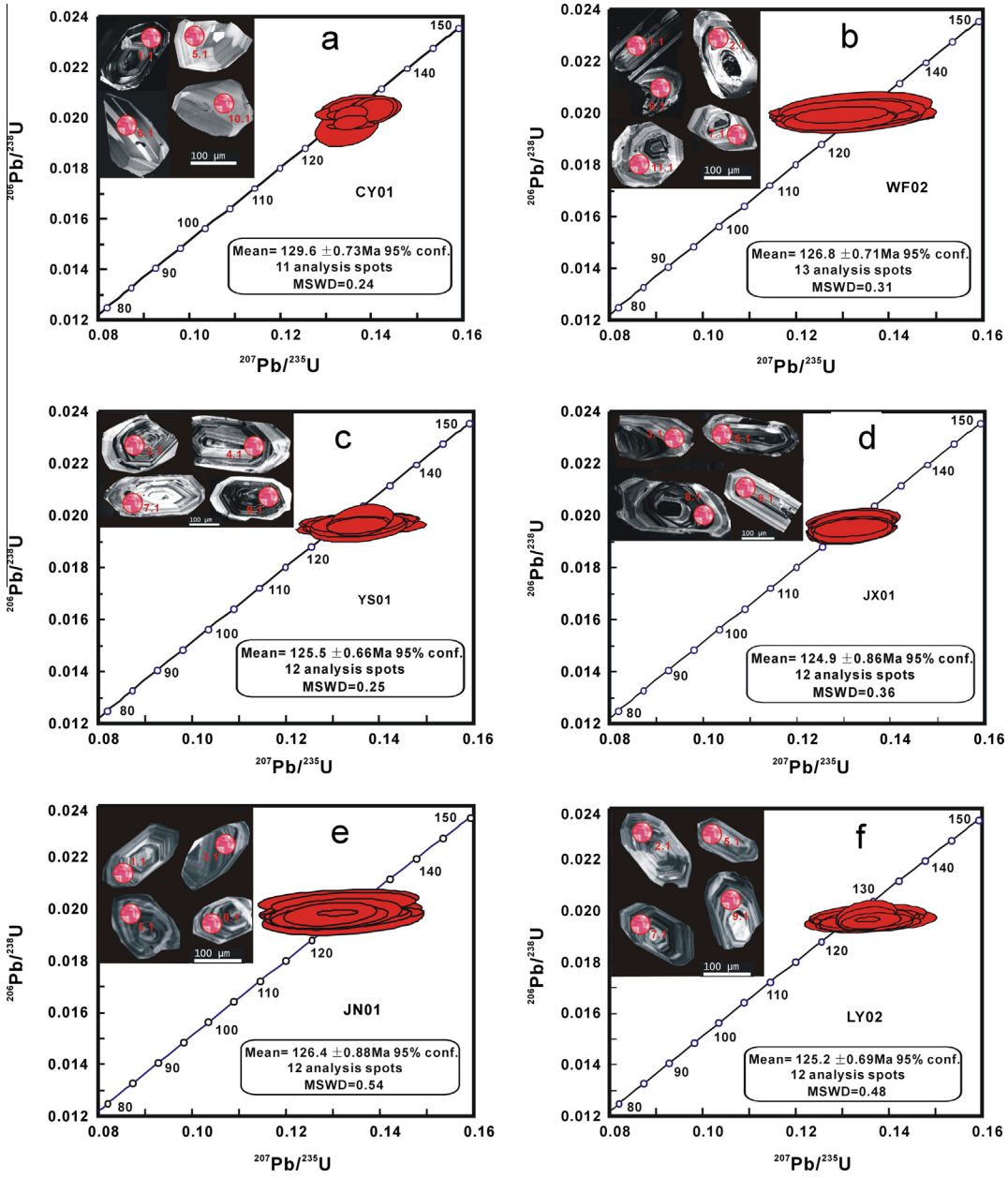

Fig. 3. Zircon LA–ICP–MS U–Pb concordia diagrams and CL images of zircons separated from the mafic dykes within the Tan–Lu Fault zone, eastern NCC, China.

and reflected light and by cathodoluminescence at the State Key Laboratory of Continental Dynamics, Northwest University, China. Prior to zircon U–Pb dating, grain mount surfaces were washed in dilute HNO_3 and pure alcohol to remove any potential lead contamination. Zircon U–Pb ages were determined by LA–ICP–MS (Table 1; Fig. 3) using an Agilent 7500a ICP–MS instrument equipped with a 193 nm excimer laser at the State Key Laboratory of Continental Dynamics, Northwest University, China. A # 91500 standard zircon was used for quality control, and a NIST 610 standard was used for data optimization. A spot diameter of 24 μm was used during analysis, employing the methodologies described by Liu et al. (2010). Common Pb correction was undertaken following the approach of Andersen (2002), and the resulting data were processed using GLITTER and ISOPLOT (Table 1; Fig. 3). Uncertainties on individual LA–ICP–MS analyses are quoted at the 95% (1σ) confidence level.

2.2. Whole-rock geochemistry

The whole-rock geochemical and Sr–Nd isotope compositions of 24 samples were determined during this study. Prior to whole-rock geochemical analysis, samples were trimmed to remove altered surfaces, cleaned with deionized water, and crushed and powdered in an agate mill. Major element concentrations were determined on fused glass disks using PANalytical Axios-advance X-ray fluorescence spectrometer at the State Key Laboratory of Ore Deposit Geochemistry, Institute of Geochemistry, Chinese Academy of Sciences, China. These analyses have a precision of <5% as determined using GSR-1 and GSR-3 Chinese national standards (Table 2). Losses on ignition values were obtained using 1 g of powder heated to 1100 °C for 1 h. Trace element concentrations were determined using ICP–MS at the State Key Laboratory of Ore Deposit Geochemistry, Institute of Geochemistry, Chinese Academy of Sciences,

Table 2
Major element concentrations (in wt.%) for the mafic dykes within the Tan–Lu Fault zone; LOI = loss on ignition, $Mg^{\#} = 100 \times Mg/(Mg + Fe)$ in atomic proportions.

Sample	Rock type	SiO_2	TiO_2	Al_2O_3	Fe_2O_3	MnO	MgO	CaO	Na_2O	K_2O	P_2O_5	LOI	Total	$Mg^{\#}$
CY1	Dolerite	51.52	0.86	14.72	9.27	0.15	9.82	7.36	2.66	2.53	0.48	0.25	99.61	68
CY2	Dolerite	51.55	0.83	14.63	9.26	0.14	9.76	7.37	2.65	2.51	0.46	0.43	99.59	68
CY3	Dolerite	51.49	0.84	14.51	9.28	0.13	9.78	7.35	2.67	2.54	0.45	0.55	99.59	68
CY4	Dolerite	51.51	0.87	14.71	9.25	0.14	9.79	7.38	2.64	2.52	0.51	0.26	99.58	68
WF1	Dolerite	51.48	0.79	14.68	9.26	0.14	9.75	7.34	2.68	2.49	0.53	0.45	99.59	68
WF2	Dolerite	51.49	0.78	14.65	9.27	0.15	9.76	7.35	2.66	2.51	0.52	0.43	99.57	68
WF3	Dolerite	51.47	0.77	14.67	9.25	0.13	9.73	7.36	2.71	2.47	0.54	0.39	99.49	68
WF4	Dolerite	51.46	0.76	14.69	9.26	0.15	9.77	7.33	2.72	2.46	0.51	0.47	99.58	68
YS1	Dolerite	51.49	0.77	14.68	9.29	0.14	9.75	7.35	2.69	2.48	0.53	0.42	99.59	68
YS2	Dolerite	51.51	0.75	14.66	9.25	0.13	9.74	7.34	2.71	2.45	0.49	0.53	99.56	68
YS3	Dolerite	51.48	0.76	14.67	9.27	0.13	9.76	7.32	2.67	2.46	0.55	0.45	99.52	68
YS4	Dolerite	51.52	0.76	14.65	9.26	0.14	9.75	7.36	2.68	2.44	0.48	0.53	99.57	68
JX1	Dolerite	51.53	0.74	14.64	9.25	0.15	9.76	7.35	2.72	2.45	0.47	0.49	99.55	68
JX2	Dolerite	51.51	0.75	14.65	9.24	0.12	9.75	7.33	2.73	2.43	0.48	0.55	99.54	68
JX3	Dolerite	51.48	0.74	14.69	9.28	0.14	9.74	7.31	2.66	2.47	0.53	0.47	99.51	68
JX4	Dolerite	51.47	0.76	14.72	9.26	0.13	9.72	7.29	2.68	2.45	0.55	0.45	99.48	68
JN1	Dolerite	51.53	0.73	14.66	9.27	0.13	9.75	7.34	2.74	2.43	0.46	0.53	99.57	68
JN2	Dolerite	52.21	0.67	14.62	9.24	0.12	9.69	7.31	2.75	2.46	0.43	0.28	99.78	67
JN3	Dolerite	51.51	0.77	14.67	9.25	0.13	9.74	7.32	2.74	2.42	0.46	0.56	99.57	68
JN4	Dolerite	52.18	0.71	14.58	9.22	0.12	9.72	7.33	2.72	2.43	0.45	0.29	99.75	68
LY1	Dolerite	52.17	0.73	14.55	9.24	0.13	9.75	7.28	2.69	2.38	0.46	0.36	99.74	68
LY2	Dolerite	52.15	0.75	14.52	9.26	0.14	9.77	7.31	2.67	2.35	0.49	0.32	99.73	68
LY3	Dolerite	51.51	0.74	14.65	9.26	0.12	9.68	7.33	2.73	2.41	0.47	0.67	99.57	67
LY4	Dolerite	51.52	0.75	14.66	9.27	0.13	9.76	7.34	2.71	2.41	0.46	0.65	99.66	68
GSR-3	RV	44.64	2.37	13.83	13.4	0.17	7.77	8.81	3.38	2.32	0.95	2.24	99.88	
GSR-3	MV	44.75	2.36	14.14	13.35	0.16	7.74	8.82	3.18	2.3	0.97	2.12	99.89	
GSR-1	RV	72.83	0.29	13.4	2.14	0.06	0.42	1.55	3.13	5.01	0.09	0.7	99.62	
GSR-1	MV	72.65	0.29	13.52	2.18	0.06	0.46	1.56	3.15	5.03	0.11	0.69	99.70	

China, following the procedures outlined in Qi et al. (2000). Triplicate analyses were reproducible to within 5% for all elements, and analyses of the OU-6 and GBPG-1 international standards agree with recommended values (Table 3).

2.3. Sr–Nd isotope analyses

Sample powders used for Rb–Sr and Sm–Nd isotope analysis were spiked with mixed isotope tracers, dissolved in Teflon capsules using HF and HNO_3 acids, and separated using conventional cation-exchange techniques. Isotopic measurements were performed using a Finnigan Triton Ti thermal ionization mass spectrometer at the State Key Laboratory of Ore Deposit Geochemistry, Chinese Academy of Sciences, China. Procedural blanks yielded concentrations of <200 pg for Sm and Nd and <500 pg for Rb and Sr, and mass fractionation corrections for Sr and Nd isotopic ratios were based on $^{86}Sr/^{88}Sr = 0.1194$ and $^{146}Nd/^{144}Nd = 0.7219$, respectively. Analysis of the NBS987 and La Jolla standards yielded values of $^{87}Sr/^{86}Sr = 0.710246 \pm 16$ (2σ), and $^{143}Nd/^{144}Nd = 0.511863 \pm 8$ (2σ), respectively.

3. Results

3.1. Zircon LA–ICP–MS U–Pb ages

Euhedral zircon in samples CY01, WF02, YS01, JX01, JN01, and LY02 are clean and prismatic and contain clear oscillatory magmatic zoning (Fig. 3). Eleven zircons from sample CY01 yielded a weighted mean $^{206}Pb/^{238}U$ age of 129.6 ± 0.7 Ma (1σ, 95% confidence interval; Table 1; Fig. 3a), with thirteen zircons from sample WF02 yielding a weighted mean $^{206}Pb/^{238}U$ age of 126.8 ± 0.7 Ma (1σ; 95% confidence interval; Table 1; Fig. 3b), twelve zircons from sample YS01 yielding a weighted mean $^{206}Pb/^{238}U$ age of 125.5 ± 0.7 Ma (1σ; 95% confidence interval; Table 1; Fig. 3c), twelve zircons from sample JX01 yielding a weighted mean $^{206}Pb/^{238}U$ age of 124.9 ± 0.9 Ma (1σ; 95% confidence interval; Table 1; Fig. 3d), twelve zircons from sample JN01 yielding a weighted mean $^{206}Pb/^{238}U$ age of 126.4 ± 0.9 Ma (1σ; 95% confidence interval; Table 1; Fig. 3e), and twelve zircons from sample LY02 yielding a weighted mean $^{206}Pb/^{238}U$ age of 125.2 ± 0.7 Ma (1σ; 95% confidence interval; Table 1; Fig. 3f). These new data provide the best estimates of the crystallization ages of the mafic dykes within the study area, and no inherited zircons were observed in either sample population.

3.2. Major and trace element geochemistry

The whole-rock geochemical compositions of the mafic dykes sampled during this study are listed in Tables 2 and 3. These dykes have relatively uniform compositions, with SiO_2 = 51.46–52.21 wt.%, TiO_2 = 0.67–0.87 wt.%, Al_2O_3 = 14.51–14.72 wt.%, Fe_2O_3 = 9.24–9.29 wt.%, MnO = 0.12–0.15 wt.%, MgO = 9.68–9.82 wt.%, CaO = 7.29–7.38 wt.%, Na_2O = 2.64–2.74 wt.%, K_2O = 2.35–2.54 wt.%, and P_2O_5 = 0.45–0.55 wt.%. These dykes have similar compositions to other dykes from Shandong Province (Guo et al., 2004, 2005a,b; Liu et al., 2008a,b, 2009a, 2012), are all classified as alkaline on a total alkali–silica diagram (Fig. 4a), and are classified as shoshonitic on an Na_2O vs. K_2O diagram (Fig. 4b). MgO positively correlates with TiO_2 (Fig. 5e) but poorly correlates with other major oxides, such as SiO_2, Al_2O_3, $Na_2O + K_2O$, CaO, Fe_2O_3, MnO, and P_2O_5 (see Fig. 5a–d, f–h), and are enriched in light rare earth elements and depleted in heavy rare earth elements, with a wide and high range in $(La/Yb)_N$ (14.5–36.0) and a narrow spread in δEu (0.70–0.91) values (Table 3; Fig. 6a and b). In addition, these mafic dykes are enriched in large ion lithophile elements (e.g., Ba, U, K, and Pb) and have clear negative Nb, Ta, P, and Ti anomalies in primitive-mantle-normalized multi-element variation diagrams (Fig. 6a and b).

3.3. Sr–Nd isotopes

The Sr–Nd isotopic compositions of 18 representative mafic samples from the study area were determined during this study (Table 4). These dykes have a relatively narrow range of ($^{87}Sr/^{86}Sr$)

Table 3
Trace element compositions (in ppm) of the mafic dykes from the Tan–Lu Fault zone; chondrite-normalization factors used to calculate $(La/Yb)_N$ values are from Sun and McDonough (1989) and $Eu/Eu = Eu_N/\sqrt{(Sm_N \times Gd_N)}$.

Sample	Cr	Ni	Rb	Sr	Y	Zr	Nb	Ba	La	Ce	Pr	Nd	Sm	Eu
CY1	506	154	48.4	987	19.6	221	7.32	2242	65.6	133	15.4	53.8	8.42	2.12
CY2	121	68.6	62.5	1293	23.5	275	9.86	4312	92.3	195	22.1	76.8	13.2	2.98
CY3	566	233	52.6	652	17.5	142	5.93	1551	32.4	54.2	7.16	31.2	5.42	1.43
CY4	525	128	51.9	1124	19.2	186	6.54	3016	64.1	131	14.2	49.4	7.63	1.92
WF1	372	73.7	63.2	675	24.3	164	5.16	1424	55.3	91.8	13.1	44.2	7.16	1.85
WF2	451	135	58.5	1164	19.1	218	7.13	2511	72.5	138	16.4	54.5	8.15	2.12
WF3	368	78.6	73.6	727	32.3	173	5.45	1732	59.4	97.6	14.3	52.4	8.76	2.23
WF4	284	57.5	84.3	592	37.6	176	5.59	1728	55.2	98.2	13.1	46.5	7.55	1.96
YS1	66.4	53.9	74.5	1681	23.4	254	9.92	7643	97.4	195	22.2	79.3	12.8	2.78
YS2	585	165	39.3	1157	19.5	178	6.74	3865	64.6	124	15.3	50.8	7.78	1.83
YS3	322	59.5	96.2	696	16.5	166	5.48	2152	47.5	94.3	12.4	42.2	6.87	1.76
YS4	278	98.5	85.8	1051	25.2	263	7.67	3393	58.7	118	15.3	53.5	9.13	2.44
JX1	266	93.6	126	868	26.4	271	8.04	2964	61.6	125	15.5	56.4	9.45	2.45
JX2	264	85.8	76.7	962	26.5	275	7.85	2126	62.5	126	15.3	56.5	9.65	2.46
JX3	163	66.5	131	753	27.6	292	8.43	4853	66.4	118	16.1	57.4	9.82	2.42
JX4	237	82.7	138	985	26.3	274	8.32	2576	62.3	124	15.4	55.3	9.43	2.37
JN1	176	65.6	94.5	864	28.4	286	8.54	3815	66.5	135	16.2	58.7	10.5	2.62
JN2	292	107	128	976	25.5	261	7.93	2473	59.6	119	15.3	53.4	8.97	2.44
JN3	315	122	143	978	26.1	253	9.44	2852	67.1	134	16.2	58.6	9.87	2.45
JN4	274	84.6	73.6	869	25.3	272	8.13	2605	64.2	126	15.2	56.4	9.32	2.42
LY1	263	83.5	85.7	1054	26.2	278	8.64	1283	64.5	128	16.3	57.6	9.64	2.48
LY2	181	76.3	121	981	24.3	255	8.28	1471	53.1	106	13.1	48.4	8.31	2.22
LY3	287	114	123	969	25.6	248	8.24	2445	58.6	118	14.3	53.2	8.94	2.54
LY4	236	82.9	154	1142	27.4	291	8.93	3353	63.3	127	15.4	56.8	9.54	2.53
OU-6 (RV)	70.8	39.8	120	131	27.4	174	14.8	477	33	74.4	7.8	29	5.92	1.36
OU-6 (MV)	73.5	42.5	122	136	26.2	183	15.3	486	33.1	78	8.09	30.6	5.99	1.35
GBPG-1 (RV)	181	59.6	56.2	364	26.2	183	9.93	908	53	103	1.15	43.3	6.79	1.79
GBPG-1 (MV)	187	60.6	61.4	377	18	232	8.74	921	51	105	1.16	42.4	6.63	1.69

Gd	Tb	Dy	Ho	Er	Tm	Yb	Lu	Hf	Ta	Pb	Th	U	$(La/Yb)_N$	δEu
6.24	0.85	4.13	0.82	2.13	0.32	1.93	0.29	4.52	0.14	12.1	12.2	4.53	24.4	0.86
9.65	1.16	5.05	0.91	2.42	0.33	1.96	0.32	5.13	0.15	22.3	14.3	2.65	33.8	0.77
4.87	0.65	3.43	0.76	1.95	0.27	1.71	0.26	3.21	0.13	21.6	5.95	1.56	13.6	0.83
6.45	0.82	3.82	0.81	2.14	0.29	1.79	0.28	3.93	0.12	13.3	9.12	1.14	25.7	0.81
6.16	0.84	4.11	0.85	2.22	0.31	1.75	0.28	3.54	0.11	4.95	7.26	1.32	22.7	0.83
6.42	0.83	3.83	0.83	2.11	0.28	1.78	0.27	4.43	0.13	11.5	12.8	1.63	29.2	0.86
7.55	0.98	5.45	1.13	3.21	0.45	2.93	0.46	3.76	0.12	6.66	7.95	1.65	14.5	0.82
6.78	0.92	5.18	1.12	3.08	0.42	2.54	0.38	3.75	0.11	6.94	8.18	1.54	15.6	0.82
10.8	1.15	4.96	0.94	2.44	0.32	1.94	0.31	5.15	0.15	25.5	15.4	2.91	36.0	0.70
6.74	0.81	3.84	0.75	2.15	0.28	1.85	0.28	4.14	0.12	14.4	9.75	1.32	25.0	0.75
5.45	0.73	3.42	0.64	1.76	0.24	1.54	0.24	3.83	0.11	7.65	7.85	1.43	22.1	0.85
8.18	0.96	4.91	0.96	2.63	0.35	2.12	0.34	5.16	0.52	23.2	5.76	1.85	19.9	0.84
8.54	0.98	5.13	0.95	2.72	0.37	2.33	0.35	5.45	0.53	24.5	6.06	3.98	19.0	0.82
7.96	0.97	5.15	0.97	2.73	0.36	2.41	0.36	5.43	0.55	29.6	5.83	2.86	18.6	0.83
9.06	1.12	5.55	1.11	2.92	0.37	2.54	0.38	5.76	0.54	41.6	5.82	1.55	18.8	0.77
8.22	0.97	5.14	0.96	2.74	0.36	2.33	0.35	5.32	0.55	26.5	5.94	2.92	19.2	0.80
8.93	1.13	5.72	1.14	2.93	0.38	2.42	0.38	5.83	0.57	55.4	6.23	2.98	19.7	0.81
7.83	0.94	4.94	0.95	2.64	0.35	2.31	0.34	5.15	0.53	18.7	5.51	1.33	18.5	0.87
8.55	0.98	5.35	0.97	2.67	0.36	2.36	0.36	5.22	0.62	21.1	8.98	1.95	20.4	0.80
7.86	0.95	5.16	0.96	2.63	0.36	2.32	0.36	5.43	0.64	21.4	5.95	3.63	19.8	0.84
7.85	1.05	5.43	0.98	2.82	0.35	2.43	0.37	5.45	0.65	29.3	5.81	2.72	19.0	0.84
6.74	0.94	5.66	0.92	2.43	0.36	2.14	0.32	4.93	0.66	29.2	5.76	2.55	17.8	0.88
7.73	0.95	4.93	0.94	2.64	0.35	2.21	0.33	5.12	0.67	19.4	5.45	1.33	19.0	0.91
8.75	0.96	5.35	0.98	2.82	0.38	2.32	0.36	5.54	0.69	22.6	5.92	2.55	19.6	0.83
5.27	0.85	4.99	1.01	2.98	0.44	3	0.45	4.7	1.06	28.2	11.5	1.96		
5.5	0.83	5.06	1.02	3.07	0.46	3.09	0.47	4.86	1.02	32.7	13.9	2.19		
4.74	0.6	3.26	0.69	2.01	0.3	2.03	0.31	6.07	0.4	14.1	11.2	0.9		
4.47	0.59	3.17	0.66	2.02	0.29	2.03	0.31	5.93	0.46	14.5	11.4	0.99		

$_i$ values (0.7099–0.7100) and have negative $\varepsilon_{Nd}(t)$ values (−14.4 to −13.7; Table 4; Fig. 7) that are indicative of magmas sourced from an enriched region of the mantle. From Fig. 7, the mafic dykes along the Tan–Lu Fault zone fall within the field outlined for other mafic dykes in Shandong province, but are significant enriched compared to the majority of these other Shandong dykes (Guo et al., 2004, 2005a,b; Liu et al., 2008a,b, 2009a, 2012).

4. Discussion

The new zircon, geochemical, and Sr–Nd isotope data presented in this study allow us to constrain the source, crustal contamination, fractional crystallization, and evolution of the magmas that were emplaced within the Tan–Lu Fault zone of the southeastern NCC.

4.1. Source and petrogenesis

The Early Cretaceous (130–125 Ma) mafic dykes within the study area are characterized by low SiO_2 concentrations (51.5–52.2 wt.%; Table 2), suggesting that they were derived from an ultramafic source (Liu et al., 2008a,b, 2009a, 2013a,b,c,d). An ultramafic source is also supported by the relatively high MgO (9.68–9.82 wt.%), $Mg^{\#}$ values (67–68, not shown), Cr (66.4–585 ppm)

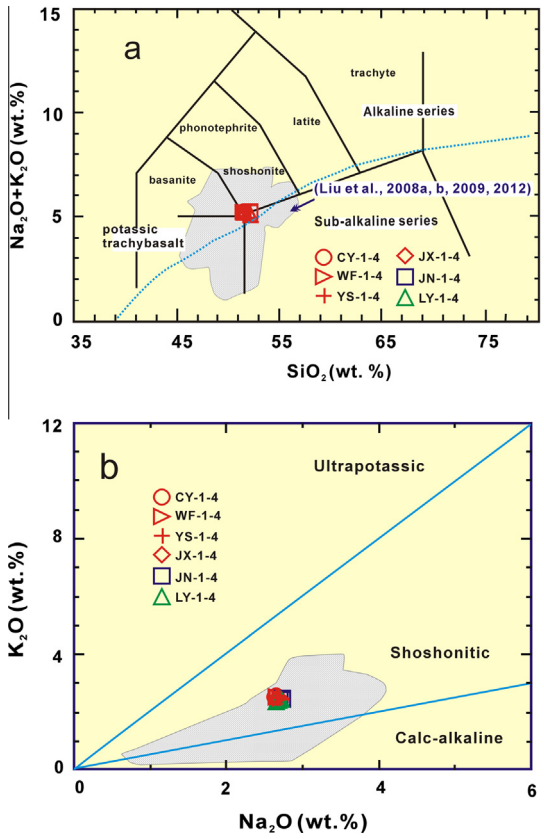

Fig. 4. Classification of the mafic dykes from the Tan–Lu Fault zone using: (a) the TAS diagram (Middlemost, 1994; Le Maitre, 2002) based on major element concentrations recalculated to 100% volatile-free compositions, and (b) the K_2O vs. Na_2O diagram (Menzies and Kyle, 1972).

and Ni (53.9–233 ppm) of these dykes (Tables 2 and 3). Further, a crustal source can be ruled out as partial melting of any crustal rocks (e.g., Hirajima et al., 1990) or lower-crustal intermediate granulites (Gao et al., 1998) would produce melts with high Si and low Mg concentrations (i.e., granitoid liquids; Rapp et al., 2003). The high initial $^{87}Sr/^{86}Sr$ ratios (0.7099–0.7100) and negative ε_{Nd} (t) values (−14.4 to −13.7; Table 4) of these dykes are consistent with an origin from an enriched lithospheric mantle source rather than from a depleted region of the mantle as in the case for MORB. In addition to the evidence outlined above, the samples analyzed during this study define a partial melting trend on La vs. La/Yb and Ni vs. Th diagrams (not shown; Liu et al., 2008c), indicating that the magmas that formed these dykes were derived from the partial melting of an enriched region of the mantle. In addition, based on the modeled calculations of Guo et al. (2014), the partial melting degree of the studied dykes ranges from 12.0% to 15.0%.

4.2. Crustal contamination and fractional crystallization

Crustal contamination can cause significant Nb–Ta depletions in basaltic rocks and can lead to mafic magmas with enriched Sr–Nd isotopic compositions (Guo et al., 2004). The dolerites within the study area are characterized by negative Nb–Ta anomalies (Fig. 6b) and have high initial $^{87}Sr/^{86}Sr$ ratios and negative ε_{Nd} (t) values (Table 4) that are indicative of the involvement of a crustal component in their petrogenesis. However, the poor correlations between SiO_2, Al_2O_3, $Na_2O + K_2O$, CaO, Fe_2O_3, MnO, and P_2O_5 and MgO (Fig. 5), and an homogeneous Sr and slight variation in Nd isotope composition, imply that there was little to no crustal contamination during the ascent of magmas, despite an absence of inheritance within zircon found within these dykes. This observation is further supported by the fact that the dykes have high Cr (66.4–585 ppm) and Ni (53.9–233 ppm) (Table 3), no correlation between $Mg^{\#}$, Cr, Ni and initial Sr ratio (not shown), distinctive negative high field strength elements (Nb, Ta, P, and Ti) and positive Pb anomalies (Fig. 6a and b; Zhang et al., 2005), high La/Nb and Ba/Nb ratios (5.0–11.0, 148–770; Table 3; Jahn et al., 1999), high $(^{87}Sr/^{86}Sr)_i$ values (0.7099–0.7100), and negative ε_{Nd} (t) values (−14.4 to −13.7; Table 4; Fig. 7).

Mafic dykes within the Tan–Lu Fault zone have quite constant MgO concentrations or high $Mg^{\#}$ values (67–68; not shown) indicating that the studied rocks experienced negligible fractional crystallization (Fig. 8). In addition, only slightly negative Eu anomalies suggests little to no plagioclase fractionation occurred prior to dyke emplacement (Table 3; Fig. 6a and b).

4.3. Genetic model and significance of the mafic dykes

The mafic dykes within the Tan–Lu Fault zone provide evidence of significant lithospheric extension during the Early Cretaceous as well as possible evidence for the evolution of the mantle beneath the study area within the southeastern NCC. As noted above, it is likely that the mafic magmas that formed the dykes were generated by melting of an enriched mantle source, although how this enriched source was formed is unclear.

At present, a significant number of Mesozoic dykes have been discovered within Shandong Province (including in the area of the Tan–Lu Fault zone; e.g., 120–128 Ma, Yang et al., 2004; 115–127 Ma, Guo et al., 2004, 2014; 89–170 Ma, Liu et al., 2004, 2005, 2006, 2008a,b,c, 2009a, 2012, 2013a,b,c,d,e; Ma et al., 2014a,b). Studies of these dykes indicate that almost all of the Mesozoic mafic dykes from Shandong Province were derived from enriched mantle source; however, the extent of this enrichment differs between western Shandong and eastern Shandong (relative enrichment with respect to Sr–Nd isotopes) and over time (i.e., from Triassic to Cretaceous, the mafic dykes have a progressively higher initial Sr isotopic ratio, and lower ε_{Nd} (t)). Moreover, five main genetic models have been proposed for these dykes: (1) derivation from a lithospheric mantle that was previously metasomatized by subduction zone processes (Yang et al., 2004); (2) decompression melting of an enriched mantle source that was mainly composed of phlogopite garnet peridotite, together with strong fractional crystallization (Guo et al., 2004); (3) derivation from the "cold" subduction of the Yangtze Craton (Guo et al., 2014); (4) delamination of eclogitic lower crust (Liu et al., 2008a,b,c, 2009a, 2012, 2013a,b,c,d,e), and (5) interaction of subducted sediment melts and the Palaeozoic lithospheric mantle of the NCC (Ma et al., 2014a). In these models, model 1, 2, and 5 all dealt with the source of the dykes that were generally hybridized by crustal material or sedimentary rock. In the source region, three models can be applicable; however, they are not fully supported by the geological record nor our data. Thus, we should discuss the other two possibilities.

The studied dykes exhibit arc-like trace element characteristics, including light rare earth element and large ion lithophile element enrichment, slightly negative Eu and Nb–Ta–P–Ti anomalies, positive Th–U anomalies, and EM_2-type Sr–Nd isotopic compositions (Zhang and Sun, 2002; Guo et al., 2013a,b); however, based on our observations and data outlined above (see Section 4.2), no crustal contamination during the ascent of magmas is evident. In general, if delamination of eclogitic lower crust occurred, this would lead to rapid uplift of the study area (Menzies et al., 2007). Evidence for this uplift is lacking, however. At the same time, lithospheric delamination would induce asthenospheric upwelling, leading to decompression melting and the formation and eruption of basalt with similar geochemical features to that

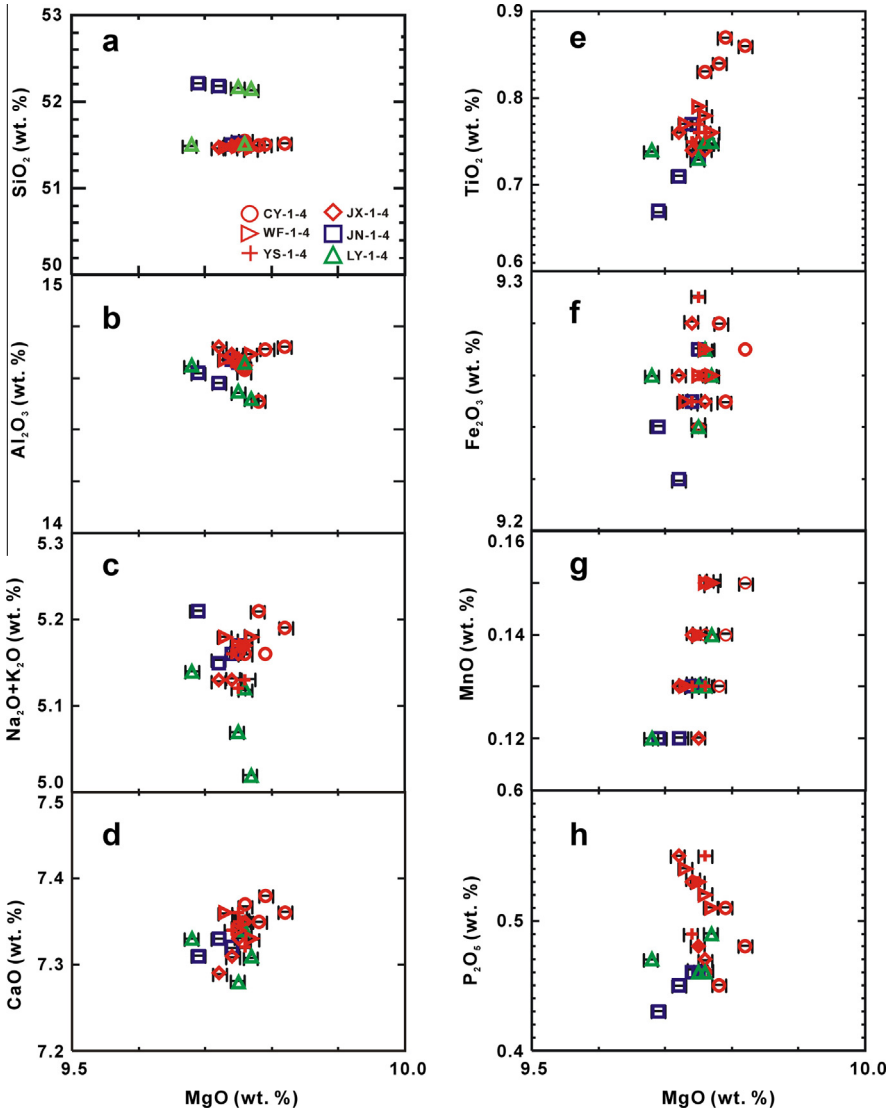

Fig. 5. Variations in major element concentrations compared to MgO (in wt.%) for the mafic dykes of the Tan–Lu Fault zone, southeastern NCC, China.

of MORB or OIB. The absence of such asthenospherically-derived magma contemporaneous with the studied dykes thus argues against a delamination of the lithosphere, in the southeastern NCC. Furthermore, new oxygen isotope data for olivine within the Fangcheng basalts, NCC, that have similar Sr–Nd isotope data to the studied dykes (Guo et al., 2013a,b), indicate the involvement of upper-middle crustal rather than lower crustal components in the melting source region for the Fangcheng basalts. As such, an alternative model is needed to account for the formation of the Tan–Lu Fault zone mafic dykes.

Important questions in the study of the Tan–Lu Fault zone mafic dykes, are what is the cause of the enriched mantle source to the mafic magmas, and where do the hybridized materials derive? These key issues will be discussed next. By contrast with the exposed Archaean–Proterozoic metamorphic complexes and typical marine sediment as a possible explanation, Guo et al. (2014) sought help from "cold" subduction of the Yangtze Craton to explain the origin of the mafic dykes (115 Ma) from Jiaodong peninsula. Their interpretation has provided credible evidence, based on which, we propose that a sedimentary component derived from Yangtze Craton, continental crust to be the cause of mantle enrichment beneath the study area. The interaction of sedimentary melt with overlying mantle lithologies helped to generate fertile mantle pyroxenite. Partial melting of this modified, and olivine-poor, pyroxenite can produce Mg-rich magmas with high Cr–Ni and low Nb–Ta–P–Ti concentrations. In the Guo et al. (2014) study, it was indeed suggested that fertile pyroxenite, formed through sediment melt–peridotite interaction, to be the source of mafic dykes emplaced along the Tan–Lu Fault (Guo et al., 2014). In accordance with geophysical observations (Engebretson et al., 1985), oblique subduction of the paleo-Pacific Plate toward the NCC occurred during the Early Cretaceous. This subduction exerted a driving force to induce the extensive collapse of the southeastern margin of the NCC, triggering extensive melting of the metasomatized mantle responsible for mafic magmatism across the NCC (Wu et al., 2005).

As such, a special model can explain the formation of the mafic dykes within the Tan–Lu Fault zone. Chemenda et al. (2002) proposed a two-dimensional thermo-mechanical, laboratory model for continental subduction, and used this to interpret the evolutionary history of the India-Asia collisional system. They suggested that subducted continental crust or sediments would be detached from underlying lithosphere mantle if the subduction was sufficiently rapid or if the subducted lithosphere had a thick lower crust (Zhang and Sun, 2002). This model may be suitable for the Triassic,

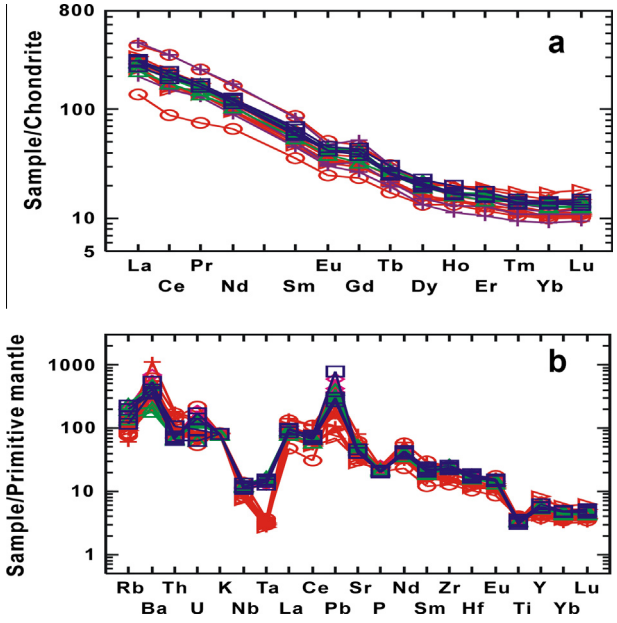

Fig. 6. Chondrite-normalized REE (a) and primitive-mantle-normalized multi-element variation diagrams (b) for the mafic dykes within the Tan–Lu Fault zone of the southeastern NCC, China. Concentrations are normalized to the chondrite composition of Sun and McDonough (1989).

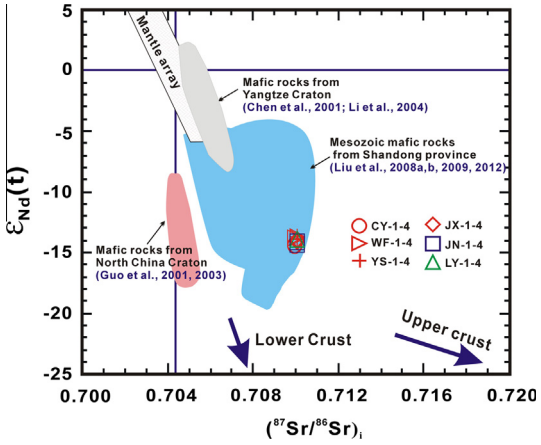

Fig. 7. Variations in initial $^{87}Sr/^{86}Sr$ and ε_{Nd} (t) values for the mafic dykes from the Tan–Lu Fault zone of the southeastern NCC, China. This diagram also includes a field delineating the composition of Mesozoic mafic dykes within the Yangtze Craton, the NCC, the Sulu Belt, and other areas within Shandong Province (Chen et al., 2001; Guo et al., 2001, 2003, 2004, 2005a,b; Li et al., 2004; Liu, 2004; Liu et al., 2008a,b, 2009a,b, 2012). The mafic dykes analyzed during this study plot within the enriched mantle source field.

Dabie collisional zone because the Yangtze Craton is an old Craton and should have had a thickened lower crust. Thus, we adopt this explanation to help reconstruct possible scenarios for the Dabie collision and for the formation of the Mesozoic lithosphere adjacent to the Dabie Orogen.

At ~240 Ma, collision between the Yangtze Craton and the NCC occurred along with northward subduction of the paleo-Tethys oceanic lithosphere (Zhang and Sun, 2002). The Yangtze lithosphere was dragged down into mantle by the denser oceanic lithosphere it comprised. Subsequently, the upper/middle Yangtze crust and sedimentary drape reached a depth of ~200 km (Ye et al., 2000; Zhang and Sun, 2002) and subsequently rapidly moved upward between the NCC and Yangtze Craton in response to slab break-off of the subducting oceanic lithosphere (Davies et al., 1995; O'Brien, 2001). At ~220 Ma, Yangtze subduction switched to a highly compressional mode (Chemenda et al., 2002), which resulted in the detachment of the Yangtze crust and sediments from the mantle. The crust would be then tectonically underplated beneath the base of the NCC lithosphere because of its buoyancy relative to the surrounding mantle. This process would lead to a thickened continental root and an isostatic uplift of the southeastern NCC. The thickened continental root was then probably eclogitized (Leech, 2001) or melted (Skjerlie and Douge, 2002) by underlying asthenosphere.

Subsequently, silicic melts produced by melting of these crustal materials migrated through the overriding continental lithosphere and interacted with mantle peridotite. Extensive interaction would have completely destroyed the old lithosphere regime, finally generating the Sr–Nd isotopic enriched (hybridized) Mesozoic lithosphere that was the source for the Cretaceous dykes' intrusion. As a result, decompression melting of this enriched mantle at 130–120 Ma produced primary basaltic melts that evolved to form the mafic magmas that were emplaced as swarms of dykes across the Tan–Lu Fault zone of the southeastern NCC.

Table 4
Sr–Nd isotopic compositions of the mafic dykes from the Tan–Lu Fault zone of the southeastern NCC calculated using Chondrite Uniform Reservoir values and decay constants of $\lambda_{Rb} = 1.42 \times 10^{-11}$ year^{-1} (Steiger and Jäger, 1977) and $\lambda_{Sm} = 6.54 \times 10^{-12}$ year^{-1} (Lugmair and Harti, 1978).

Sample	Rb (ppm)	Sr (ppm)	$^{87}Rb/^{86}Sr$	$^{87}Sr/^{86}Sr$	±2σ	Sm (ppm)	Nd (ppm)	$^{147}Sm/^{144}Nd$	$^{143}Nd/^{144}Nd$	±2σ	$(^{87}Sr/^{86}Sr)_i$	$(^{143}Nd/^{144}Nd)_i$	ε_{Nd} (t)
CY1	48.4	987	0.142	0.710205	13	8.42	53.8	0.0946	0.511816	8	0.709944	0.511736	−14.4
CY2	62.5	1293	0.140	0.710193	13	13.2	76.8	0.1039	0.511821	8	0.709944	0.511733	−14.4
CY3	52.6	652	0.233	0.710362	16	5.42	31.2	0.1050	0.511826	12	0.709935	0.511737	−14.3
WF2	58.5	1164	0.145	0.710288	13	8.15	54.5	0.0904	0.511843	10	0.709932	0.511768	−13.8
WF3	73.6	727	0.293	0.710381	14	8.76	52.4	0.1011	0.511855	9	0.710026	0.511771	−13.7
WF4	84.3	592	0.412	0.710771	14	7.55	46.5	0.0982	0.511848	9	0.710028	0.511767	−13.8
YS1	74.5	1681	0.128	0.710263	12	12.8	79.3	0.0976	0.511844	10	0.710034	0.511764	−13.9
YS3	96.2	696	0.400	0.710741	13	6.87	42.2	0.0984	0.511853	10	0.710028	0.511772	−13.7
YS4	85.8	1051	0.236	0.710453	16	9.13	53.5	0.1032	0.511847	8	0.710032	0.511762	−13.9
JX1	126.0	868	0.420	0.710776	13	9.45	56.4	0.1013	0.511847	10	0.710030	0.511764	−13.9
JX2	76.7	962	0.231	0.710438	13	9.65	56.5	0.1032	0.511846	9	0.710028	0.511762	−14.0
JX4	138.0	985	0.405	0.710764	14	9.43	55.3	0.1031	0.511841	9	0.710044	0.511757	−14.1
JN1	94.5	864	0.317	0.710613	13	10.5	58.7	0.1081	0.511833	12	0.710044	0.511744	−14.3
JN2	128	976	0.380	0.710725	16	8.97	53.4	0.1015	0.511835	10	0.710043	0.511751	−14.1
JN3	143	978	0.423	0.710793	13	9.87	58.6	0.1018	0.511838	10	0.710033	0.511754	−14.1
LY1	85.7	1054	0.235	0.710452	16	9.64	57.6	0.1012	0.511845	10	0.710033	0.511762	−13.9
LY2	121	981	0.357	0.710674	13	8.31	48.4	0.1038	0.511848	9	0.710039	0.511763	−13.9
LY4	154	1142	0.390	0.710732	13	9.54	56.8	0.1015	0.511847	9	0.710038	0.511764	−13.9

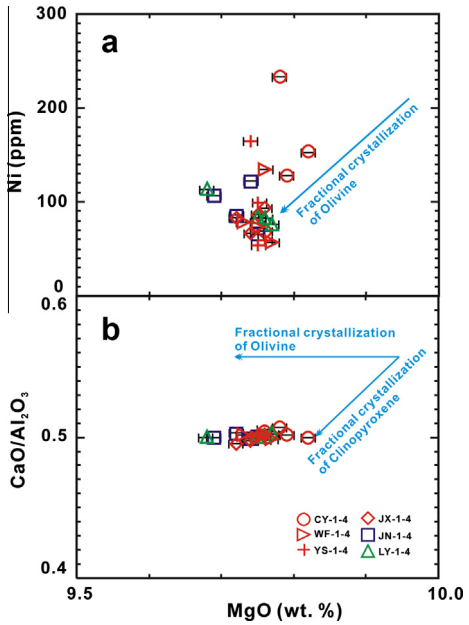

Fig. 8. Ni (in ppm) (a) and CaO/Al_2O_3 (b) vs. MgO (in wt.%) diagrams for the mafic dykes from the Tan–Lu Fault, southeastern NCC.

5. Conclusions

The new geochronological, geochemical, and Sr–Nd isotopic data for the mafic dykes within the Tan–Lu Fault zone of the southeastern NCC allow the following conclusions to be reached.

1. Zircon U–Pb dating indicates that the mafic dykes within the Tan–Lu Fault zone of the southeastern NCC were emplaced 129.6 ± 0.7 Ma, 125.2 ± 0.7 Ma, 125.5 ± 0.7 Ma, 124.9 ± 0.9 Ma, 126.4 ± 0.9 Ma, and 126.8 ± 0.7 Ma (i.e., during the Early Cretaceous).
2. The mafic dykes in the study area are alkaline and shoshonitic (Fig. 4a and b), have high and variable light rare earth element concentrations with slight negative Eu anomalies (δEu = 0.70–0.91), and have positive Ba, U, K, and Pb, and negative Nb, Ta, P, and Ti anomalies (Fig. 6a and b). These dykes were derived from partial melting (partial melting degree: 12.0–15.0%) of an enriched mantle source ($(^{87}Sr/^{86}Sr)_i$ values = 0.7099–0.7100, $\varepsilon_{Nd}(t)$ values = −14.4 to −13.7), and formed from parental magmas that were generated during lithospheric extension-related partial melting of an enriched region of the lithospheric mantle beneath the southeastern NCC. These parental magmas fractionated out olivine and Fe–Ti oxides, such as rutile, ilmenite, and titanite during ascent and before emplacement as mafic dykes in the study area, but did not significantly fractionate plagioclase. In addition, there were negligible crustal contamination of these magmas during emplacement.
3. The mafic dykes in the study area formed in an extensional setting following collision between the NCC and the Yangtze Craton. The magmas that formed these dykes were sourced from a hybridized source caused by subduction of Yangtze crustal sedimentary material beneath NCC, or by subduction of the paleo-Pacific Plate before the late Mesozoic.

Acknowledgements

This research was supported by the Opening Project (201206) of the State Key Laboratory of Ore Deposit Geochemistry, and by the National Natural Science Foundation of China (41373028). The authors thank Lian Zhou and Xiaoming Liu for assistance during zircon U–Pb dating and Sr–Nd isotope analysis. In addition, the efforts of editor in chief (Prof. Bor-ming Jahn) and anonymous reviewers are also much appreciated.

References

Andersen, T., 2002. Correction of common lead in U–Pb analyses that do not report ^{204}Pb. Chem. Geol. 192, 59–79.
Chemenda, A.I., Burg, J.P., Mattauer, M., 2002. Evolutionary model of the Himalaya–Tibet system: Geopoem based on new modeling, geological, and geophysical data. Earth Planet. Sci. Lett. 174, 397–409.
Chen, J.F., Yan, J., Xie, Z., Xu, X., Xing, F.M., 2001. Nd and Sr isotopic compositions of igneous rockis from the Lower Yangtze region in eastern China: Constraints on sources. Phys. Chem. Earth. (A) 26, 719–731.
Chen, L., Sunm, Y., Diwu, C.R., Wang, H.L., 2009. Crust formation in the Ordos block: Constraints from detrital zircons from Ordovican and Permian sandstones. In: Abstract with Program of International Discussion meeting on Continental Geology and Tectonics. Northwest University Press, Xi'an, p. 17.
Davies, J.H., Von, Blanckenburg., F., 1995. Slab breakoff: a model of lithosphere detachment and its test in the magmatism and deformation of collisional orogens. Earth Planet. Sci. Lett. 129, 85–102.
Diwu, C.R., Sun, Y., Yuan, H.L., Wang, H.L., Zhong, X.P., Liu, X.M., 2008. Detrital zircon U–Pb chronology, Hf isotopic compositions and geological significance of Songshan quartzites from Dengfeng, Henan. Chin. Sci. Bull. 53, 1923–1934 (in Chinese).
Engebretson, D.C., Cox, A., Gordon, R.G., 1985. Relative motions between oceanic and continental plates in the Pacific basins. Geol. Soc. Am. Special Paper 206, 1–59.
Gao, S., Zhang, B.R., Jin, Z.M., Kern, H., Luo, T.C., Zhao, Z.D., 1998. How mafic is the lower continental crust? Earth Planet. Sci. Lett. 106, 101–117.
Gao, L.Z., Zhao, T., Wang, Y.S., Zhao, X., Ma, Y.S., Yang, S.Z., 2005. Zircon U–Pb SHRIMP ages of Precambrian basement in Yuntai Mountains, Jiaozuo, Henan. Geol. Bull. China 24, 1089–1093 (in Chinese w ith English abstract).
Guo, F., Fan, W.M., Wang, Y.J., Lin, G., 2001. Late Mesozoic mafic intrusiive complexes in north China block: Constraints on the nature of subcontinental lithospheric mantle. Phys. Chem. Earth. (A) 26, 759–771.
Guo, F., Fan, W.M., Wang, Y.J., Lin, G., 2003. Geochemistry of late Mesozoic mafic magmatism in west Shandong province, eastern China: Charactrizing the lost lithospheric mantle beneath the North China block. Geochem. J. 40, 63–77.
Guo, F., Fan, W.M., Wang, Y.J., Zhang, M., 2004. Origin of Early Cretaceous calc-alkaline lamprophyres from the Sulu orogen in eastern China: implications for enrichment processes beneath continental collisional belt. Lithos 78, 291–305.
Guo, F., Fan, W.M., Wang, Y.J., Li, C.W., Li, X.Y., Zhang, H.F., 2005a. Geochemistry of late Mesozoic mafic rocks from the Dabie-Sulu region, China: constraints on the nature of lithospheric mantle beneath the orogen. Acta Petrol. Sin. 21, 1265–1270 (in Chinese with English abstract).
Guo, J.H., Sun, M., Chen, F.K., Zhai, M.G., 2005b. Sm–Nd and SHRIMP U–Pb zircon geochronology of high-pressure granulites in the Sanggan area, North China Craton: timing of Palaeoproterozoic continental collision. J. Asian Earth Sci. 24, 629–642.
Guo, J.T., Guo, F., Wang, C.Y., Li, C.W., 2013a. Crustal recycling processes in generating the Early Cretaceous Fangcheng basalts, North China Craton: new constraints from mineral chemistry, oxygen isotopes of olivine and whole-rock geochemistry. Lithos 170–171, 1–16.
Guo, P., Santosh, M., Li, S., 2013b. Geodynamics of gold metallogeny in the Shandong Province, NE China: an integrated geological, geophysical and geochemical perspective. Gondwana Res. 24, 1172–1202.
Guo, F., Fan, W.M., Li, C.W., Wang, C.Y., Li, H.X., Zhao, L., Li, J.Y., 2014. Hf–Nd–O isotopic evidence for melting of recycled sediments beneath the Sulu Orogen, North China. Chem. Geol. 381, 243–258.
Hirajima, T., Ishiwatari, A., Cong, B., Zhang, R., Banno, S., Nozaka, T., 1990. Coesite from Mengzhong eclogite at Donghai county, northern Jiangsu Province, China. Miner. Mag. 54, 579–583.
Hou, G.T., Liu, Y.L., Li, J.H., 2006. Evidence for 1.8 Ga extension of the Eastern Block of the North China Craton from SHRIMP U–Pb dating of mafic dyke swarms in Shandong Province. J. Asian Earth Sci. 27, 392–401.
Hou, G.T., 2012. Mafic dyke swarms of North China. Science Press, pp. 1–177(in Chinese with English abstract).
Jahn, B.M., Wu, F.Y., Lo, C.H., Tsai, C.H., 1999. Crust mantle interaction induced by deep subduction of the continental crust: geochemical and Sr–Nd isotopic evidence from post-collisional mafic–ultramafic intrusions of the northern Dabie complex, central China. Chem. Geol. 157, 119–146.
Le Maitre, R.W., 2002. Igneous Rocks: A Classification and Glossary of Terms, second ed. Cambridge University Press, Cambridge, p. 236.
Leech, M.L., 2001. Arrested orogenic development: ecologitization, delamination, and tectonic collapse. Earth Planet. Sci. Lett. 185, 149–159.
Li, Z.X., 1994. Collision between the north and south blocks: a crustal detachment model for suturing in the region east of the Tan–Lu Fault. Geology 22, 739–742.
Li, C.W., Guo, F., Li, X.Y., 2004. Geochemistry of late Mesozoic mafic volcanic rocks in Lishui basin and their tectonic implications. Geochemica 33, 361–371 (in Chinese with English abstract).

Li, J.H., He, W.Y., Qian, X.L., 1997. The genetic mechanism of mafic dyke swarm and the reconstruction of ancient plate. Geol. J. China Univ. 3, 2–8 (in Chinese with English abstract).
Liu, S., 2004. The Mesozoic magmatism and crustal extension in Shandong Province, Cina-additional discussing the relationship between lamprophyres and gold mineralization (in Chinese). In: Ph.D. thesis. Institute of Geochemistry, Chinese Academy of Sciences, Guiyang (in Chinese).
Liu, G.S., Song, C.Z., Wang, D.X., Niu, M.L., 2002. Extensional activities of the Tan–Lu Fault zone from the Late Cretaceous to the Palaeogene and its controlling for the Hefei basin. J. Hefei Univ. Technol. 25, 672–677 (in Chinese with English abstract).
Liu, S., Hu, R.Z., Zhao, J.H., Feng, C.X., 2004. K–Ar ages of Mesozoic mafic dyke rocks and crustal extension in Shandong Province, eastern China. Acta Geol. Sin. 78, 1207–1213.
Liu, S., Hu, R.Z., Zhao, J.H., Feng, C.X., Zhong, H., Cao, J.J., Shi, D.N., 2005. Geochemical characteristics and petrogenetic investigation of the late Mesozoic lamprophyres of Jiaobei, Shandong Province. Acta Petrol. Sin. 21, 947–958 (in Chinese with English abstract).
Liu, S., Zou, H.B., Hu, R.Z., Zhao, J.H., Feng, C.X., 2006. Mesozoic mafic dykes from the Shandong Peninsula, North China Craton: petrogenesis and tectonic implications. Geochem. J. 40, 181–195.
Liu, S., Hu, R.-Z., Gao, S., Feng, C.-X., Qi, L., Zhong, H., Xiao, T., Qi, Y.-Q., Wang, T., Coulson, I.M., 2008a. Zircon U–Pb geochronology and major, trace elemental and Sr–Nd–Pb isotopic geochemistry of mafic dykes in western Shandong Province, east China: constrains on their petrogenesis and geodynamic significance. Chem. Geol. 255, 329–345.
Liu, S., Hu, R., Gao, S., Feng, C., Qi, Y., Wang, T., Feng, G., Coulson, I.M., 2008b. U–Pb zircon age, geochemical and Sr–Nd–Pb–Hf isotopic constraints on age and origin of alkaline intrusions and associated mafic dikes from Sulu orogenic belt, Eastern China. Lithos 106, 365–379.
Liu, S., Hu, R.Z., Gao, S., Feng, C.X., Zhong, H., Qi, Y.Q., Wang, T., Qi, L., Feng, G.Y., 2008c. K–Ar ages and geochemical and Sr–Nd isotopic compositions of adakitic volcanic rocks, western Shandong province, eastern China: foundering of the lower continental crust. Int. Geol. Rev. 50, 763–779.
Liu, S., Hu, R., Gao, S., Feng, C., Yu, B., Feng, G., Qi, Y., Wang, T., Coulson, I.M., 2009a. Petrogenesis of Late Mesozoic mafic dykes in the Jiaodong Peninsula, eastern North China Craton and implications for the foundering of lower crust. Lithos 113, 621–639.
Liu, S., Hu, R., Gao, S., Feng, C., Yu, B., Qi, Y.Q., Wang, T., Feng, G., Coulson, I.M., 2009b. Zircon U–Pb age, geochemistry and Sr–Nd–Pb isotopic compositions of adakitic volcanic rocks from Jiaodong, Shandong Province, Eastern China: constraints on petrogenesis and implications. J. Asian Earth Sci. 35, 445–458.
Liu, Y.S., Hu, Z.C., Zong, K.Q., Gao, C.G., Gao, S., Xu, J., Chen, H.H., 2010. Reappraisement and refinement of zircon U–Pb isotope and trace element analyses by LA–ICP–MS. Chin. Sci. Bull. 55, 1535–1546.
Liu, S., Hu, R., Gao, S., Feng, C., Feng, G., Qi, Y., Coulson, I.M., Yang, Y., Yang, C., Tang, L., 2012. Geochemical and isotopic constraints on the age and origin of mafic dikes from eastern Shandong Province, eastern North China Craton. Int. Geol. Rev. 54, 1389–1400.
Liu, S., Feng, C., Jahn, B.-M., Hu, R., Gao, S., Coulson, I.M., Feng, G., Lai, S., Yang, Y., Tang, L., 2013a. Geochemical, Sr–Nd–Pb isotope, and zircon U–Pb geochronological constraints on the origin of Early Permian mafic dikes, northern North China Craton. Int. Geol. Rev. 55, 1626–1640.
Liu, S., Feng, C., Jahn, B.M., Hu, R., Gao, S., Coulson, I.M., Feng, G., Lai, S., Yang, C., Yang, Y., 2013b. Zircon U–Pb age, geochemical, and Sr–Nd–Hf isotopic constraints on the origin of mafic dykes in the Shaanxi Province, North China Craton, China. Lithos 175–176, 244–254.
Liu, S., Feng, C., Jahn, B.-M., Hu, R., Gao, S., Feng, G., Lai, S., Yang, Y., Qi, Y., Coulson, I.M., 2013c. Geochemical, Sr–Nd isotopic, and zircon U–Pb geochronological constraints on the petrogenesis of Late Paleoproterozoic mafic dykes within the northern North China Craton, Shanxi Province, China. Precamb. Res. 236, 182–192.
Liu, S., Hu, R., Gao, S., Feng, C., Coulson, I.M., Feng, G., Qi, Y., Yang, Y., Yang, C., Tang, L., 2013d. Zircon U–Pb age and Sr–Nd–Hf isotopic constraints on the age and origin of Triassic mafic dikes, Dalian area, Northeast China. Int. Geol. Rev. 55, 249–262.
Liu, S., Hu, R., Feng, C., Gao, S., Feng, G., Lai, S., Qi, Y., Coulson, I.M., Yang, Y., Yang, C., Tang, L., 2013e. U–Pb zircon age, geochemical, and Sr–Nd–Pb isotopic constraints on the age and origin of mafic dykes from eastern Shandong Province, Eastern China. Acta Geol. Sin. 87, 1045–1057.
Lugmair, G.W., Harti, K., 1978. Lunar initial $^{143}Nd/^{144}Nd$: differential evolution of the lunar crust and mantle. Earth Planet. Sci. Lett. 39, 349–357.
Luo, Z.L., Li, J.M., Li, X.J., Liu, S.G., 2005. Discussion on the formation, evolution and problem of the Tancheng–Lujiang Fault zone. J. Jilin Univ. 35, 699–706 (in Chinese with English abstract).
Ma, L., Jiang, S.Y., Hofmann, A.W., Dai, B.Z., Hou, M.L., Zhao, K.D., Chen, L.H., Li, J.W., Jiang, Y.H., 2014a. Lithospheric and asthenospheric sources of lamprophyres in the Jiaodong Peninsula: a consequence of rapid lithospheric thinning beneath the North China Craton? Geochim. Cosmochim. Acta 124, 350–371.
Ma, L., Jiang, S.Y., Hou, M.L., Dai, B.Z., Jiang, Y.H., Yang, T., Zhao, K.D., Pu, W., Zhu, Z.Y., Xu, B., 2014b. Geochemistry of early Cretaceous calc-alkaline lamprophyres in the Jiaodong Peninsula: implication for lithospheric evolution of the eastern North China Craton. Gondwana Res. 25, 859–872.
Menzies, M.A., Kyle, P.R., 1972. Continental volcanism: a crust–mantle probe. In: Menzies, M.A. (Ed.), Continental Mantle. Oxford University Press, Oxford, pp. 157–177.
Menzies, M.A., Xu, Y.G., Zhang, H.F., Fan, W.M., 2007. Integration of geology, geophysics and geochemistry: a key to understanding the North China Craton. Lithos 96, 1–21.
Middlemost, E.A.K., 1994. Naming materials in the magma/igneous rock system. Earth-Sci. Rev. 74, 193–227.
Niu, M.L., Zhu, G., Song, C.Z., 2001. Mesozoic volcanic activities and deep processes in the Tan–Lu Fault zone. J. Hefei Univ. Technol. 24, 147–153 (in Chinese with English abstract).
Niu, M.L., Zhu, G., Liu, G.S., Wang, D.X., 2002. Tectonic setting and deep processes of Mesozoic magmatism in middle-south segment of the Tan–Lu Fault. Chin. J. Geol. 37, 393–404 (in Chinese with English abstract).
Niu, M.L., Zhu, G., Liu, G.S., Song, C.Z., Wang, D.X., 2005. Cenozoic volcanic activities and deep processes in the middle-source sector of the Tan–Lu Fault zone. Chin. J. Geol. 40, 390–403 (in Chinese with English abstract).
Niu, M.L., Xie, C.L., Song, C.Z., Wang, D.X., 2007. K–Ar dating of early Cretaceous volcanic rocks along the Tan–Lu Fault zone and its tectonic significance. Chin. J. Geol. 42, 382–387 (in Chinese with English abstract).
Niu, M.L., Zhu, G., Xie, C.L., Liu, X.M., Cao, Y., Xie, W.Y., 2008. LA–ICP–MS zircon U–Pb ages of the granites from the southern segment of the Zhangbling uplift along the Tan–Lu Fault zone and their tectonic significances. Acta Petrol. Sin. 24, 1839–1847 (in Chinese with English abstract).
O'Brien, P.J., 2001. Subduction followed by collision: Alpine and Himalayan examples. Phys. Earth Planet. Interiors 127, 277–291.
Peng, P., Zhai, M.G., Zhang, H.F., Guo, J.H., 2005. Geochronological constraints on the Palaeoproterozoic evolution of the North China Craton: SHRIMP zircon ages of different types of mafic dykes. Int. Geol. Rev. 47, 492–508.
Peng, P., Zhai, M.G., Guo, J.H., Kusky, T., Zhao, T.P., 2007. Nature of mantle source contributions and crystal differentiation in the petrogenesis of the 1.78 Ga mafic dykes in the central North China Craton. Gondwana Res. 12, 29–46.
Peng, P., Zhai, M.G., Li, Z., Wu, F.Y., Hou, Q.L., 2008. Neoproterozoic (~820 Ma) mafic dyke swarms in the North China Craton: implication for a conjoint to the Rodinia supercontinent? In: Abstracts, 13th Gondwana Conference, pp. 160–161.
Peng, P., Guo, J.H., Zhai, M.G., Bleeker, W., 2010. Paleoproterozoic gabbronoritic and granitic magmatism in the northern margin of the North China Craton: evidence of crust–mantle interaction. Precamb. Res. 183, 635–659.
Peng, P., Bleeker, W., Ernst, R.E., Söderlund, U., McNicoll, V., 2011a. U–Pb baddeleyite ages, distribution and geochemistry of 925 Ma mafic dykes and 900 Ma sills in the North China Craton: evidence for a Neoproterozoic mantle plume. Lithos 127, 210–221.
Peng, P., Zhai, M.G., Li, Q.L., Wu, F.Y., Hou, Q.L., Li, Z., Li, T.S., Zhang, Y.B., 2011b. Neoproterozoic (900 Ma) Sariwon sills in North Korea: geochronology, geochemistry and implications for the evolution of the south-eastern margin of the North China Craton. Gondwana Res. 20, 243–254.
Peng, P., 2010. Reconstruction and Interpretation of Giant Mafic Dyke Swarms: A Case Study of 1.78 Ga Magmatism in the North China Craton: Geological Society Special Publication, 338. Geological Society, London, pp. 163–78.
Qi, L., Hu, J., Grégoire, D.C., 2000. Determination of trace elements in granites by inductively coupled plasma mass spectrometry. Talanta 51, 507–513.
Qian, X.F., Gao, L.Z., Peng, Y., Li, H.B., 2001. The Canghaipu earthquake in ancient Tan–Lu fault, sequence and tectonic significance. Earth China 31, 911–918.
Qiao, X.F., Gao, L.Z., Peng, Y., 2001. Canglangpu earthquake event in ancient Tan-Lu belt, sequence and tectonic significance. Sci. China (D) 31, 911–918.
Qiao, X.F., Zhang, A.D., 2002. North China block, Jiao-Liao-Korea block and Tanlu Fault. Geol. China 29, 337–345 (in Chinese with English abstract).
Rapp, R.P., Shimizu, N., Norman, M.D., 2003. Growth of early continental crust by partial melting of eclogite. Nature 425, 605–609.
Skjerlie, K.P., Douge, A.E.P., 2002. The fluid-absent partial melting of a zoisite-bearing quartz eclogite from 1.0 to 3.2 GPa: implications for melting in thickened continental crust and for subduction-zone processes. J. Petrol. 43, 291–314.
Steiger, R.H., Jäger, E., 1977. Subcommission on geochronology; convention on the use of decay constants in geochronology and cosmochronology. Earth Planet. Sci. Lett. 36, 359–362.
Sun, S.S., McDonough, W.F., 1989. Chemical and isotopic systematics of oceanic basalts: implications for mantle composition and processes. In: Saunders, A.D., Norry, M.J. (Eds.), Magmatism in the Ocean Basins. Geological Society Special Publication, Geological Society, London, pp. 313–345.
Tang, J.F., Hou, M.J., Cai, T.H., 1995. The major features and the nature discussion for the Tan–Lu Fault zone. Geol. Anhui 5, 60–65 (in Chinese with English abstract).
Wan, T.F., Zhu, H., 1996. The maximum sinistral strike-slip and its forming age of Tancheng–Lujiang Fault zone. Geol. J. Univ. 2, 14–27 (in Chinese with English abstract).
Wan, Y.S., Liu, D.Y., Song, B., 2005. Geochemical and Nd isotopic composition of 3.8 Ga meta-quartz dioritic and trondhjemitic rocks from the Archean area and their geological significance. J. Asian Earth Sci. 24, 563–575.
Wang, L.Q., Qiu, Y.M., McNaughton, N.L., Groves, D.I., Luo, Z.K., Huang, J.Z., Miao, L.C., Liu, Y.K., 1998. Constraints on crustal evolution and gold metallogeny in the northwestern Jiaodong, China, from SHRIMP U–Pb zircon studies of granitoids. Ore Geol. Rev. 13, 275–291.
Wang, X.F., Li, Z.J., Chen, B.L., 2000. Tancheng–Lujiang Fault. Geological Publishing House, Beijing, pp. 1–200, (in Chinese).
Wang, Y.S., Zhu, G., Song, C.Z., Liu, G.S., 2006. Strike-slip to extension in the Tan–Lu Fault zone on eastern terminal of the Dabie mountains. Chin. J. Geol. 41, 242–255 (in Chinese with English abstract).

Wang, H.L., Chen, L., Sun, Y., Liu, X.M., Xu, X.Y., Chen, J.L., Zhang, H., Diwu, C.R., 2007. Discovery of ca. 4.1 Ga trapped zircon. Chin. Sci. Bull. 52, 1685–1693 (in Chinese).

Wilde, S.A., Zhao, G.C., Sun, M., 2002. Development of the North China Craton during the Late Archaean and its final amalgamation at 1.8 Ga: some speculation on its position within a global Palaeoproterozoic Supercontinent. Gondwana Res. 5, 85–94.

Wu, J.S., Geng, Y.S., Shen, Q.H., Wang, Y.S., Liu, D.Y., Song, B., 1998. Archean Geological Nature and Tectonic Evolution of Sino-Korean Continent. Geology publishing House, Beijing, pp. 1–212, (in Chinese with English abstract).

Wu, F.Y., Lin, J.Q., Wilde, S.A., Zhang, X.Q., Yang, J.H., 2005. Nature and significance of the early Cretaceous giant igneous event in eastern China. Earth Planet. Sci. Lett. 233, 103–119.

Xiao, W.J., Zhou, Y.X., Yang, Z.Y., Zhao, X.X., 2000. Multiple rotation and amalganation processes of Dabie-Tanlu-Sulu orogen. Adv. Earth Sci. 15, 147–153 (in Chinese with English abstract).

Xie, C.L., Zhu, G., Niu, M.L., Wang, Y.S., 2007. LA–ICP–MS zircon U–Pb ages of the Mesozoic volcanic rocks from Chuzhou Area and their tectonic significance. Geol. Rev. 53, 642–655 (in Chinese with English abstract).

Xie, C.L., Zhu, G., Niu, M.L., Liu, X.M., 2008. Geochemistry of late Mesozoic volcanic rocks from the Chaohu-Lujiang segment of the Tan–Lu Fault zone and lithospheric thinning processes. Acta Petrol. Sin. 24, 1823–1838 (in Chinese with English abstract).

Xie, C.L., Zhu, G., Niu, M.L., Liu, X.M., 2009. Geochemistry of late Mesozoic volcanic rocks from Chuzhou area and its implication for the lithospheric thinning beneath the Tan–Lu Fault zone. Acta Petrol. Sin. 25, 92–108 (in Chinese with English abstract).

Xu, J.W., Ma, G.F., 1992. Review of ten years (1981–1991) of research on the Tancheng–Lujiang Fault zone. Geol. Rev. 38, 316–324 (in Chinese with English abstract).

Xu, J.W., Zhu, G., 1994. Tectonic models of the Tan–Lu Fault zone, eastern China. Int. Geol. Rev. 36, 771–784.

Xu, J.W., 1993. Basic characteristics and tectonic evolution of the Tancheng–Lujiang Fault zone. In: Xu, J.W. (Ed.), The Tancheng–Lujiang wrench Fault system. John Wiley & Sons Ltd., pp. 17–50.

Yan, G.H., Cai, J.H., Ren, K.X., Mu, B.L., Li, F.T., Chu, Z.Y., 2008. Nd, Sr and Pb isotopic geochemistry of late-Mesozoic alkaline-rich intrusions from the Tanlu Fault zone: evidence of the magma source. Acta Petrol. Sin. 24, 1223–1236 (in Chinese with English abstract).

Yang, J.H., Chung, S.L., Zhai, M.G., Zhou, X.H., 2004. Geochemical and Sr–Nd–Pb isotopic compositions of mafic dikes from the Jiaodong Peninsula, China: evidence for vein-plus-peridotite melting in the lithospheric mantle. Lithos 73, 145–160.

Ye, K., Cong, B.L., Ye, D.N., 2000. The possible subduction of continental material to depths greater than 300 km. Nature 407, 734–736.

Yin, A., Nie, S.Y., 1993. An indentation model for the north and south China collision and the development of the Tanlu and Honam fault system, eastern Asian. Tectonics 12, 801–813.

Zhai, M.G., Bian, A.G., 2000. The supercontinent assembling during Neoarchean and the cracking between Paleoproterozoic and Mesoproterozoic of the North China Craton. Sci. China 30, 129–137 (in chinese with English abstract).

Zhang, H.F., Sun, M., 2002. Geochemistry of Mesozoic basalts and mafic dykes, southeastern North China Craton, and Tectonic implications. Int. Geol. Rev. 44, 370–382.

Zhang, H.F., Sun, M., Zhou, X.H., Ying, J.F., 2005. Geochemical constraints on the origin of Mesozoic alkaline intrusive complexes from the North China Craton and tectonic implications. Lithos 81, 297–317.

Zhang, C.L., Liu, L., Wang, S.J., Liu, S., Dai, M.N., 2009. Detrital zircon provenance for the meta-sedimentary rocks from Kuanping Group, implication for Neo-proterozoictectonic reconstruction in Qinling Orogeny, central China. In: Abstract with program of international discussion meeting on continental geology and tectonics. Northwest University Press, Xi'an, pp. 64–66.

Zhang, K.J., 1997. North and south China collision along the eastern and southern North China margins. Tectonophysics 170, 145–156.

Zhao, G.C., Wilde, S.A., Cawood, P.A., Sun, M., 2001. Archean blocks and their boundaries in the North China Craton: lithological, geochemical, structural and P-T path constraints and tectonic evolution. Precamb. Res. 107, 45–73.

Zhao, G.C., Sun, M., Wilde, S.A., Li, S.Z., 2005. Late Archaean to Palaeoproterozoic evolution of the North China Craton: key issues revisited. Precamb. Res. 136, 177–202.

Zhao, G.C., 2014. Precambrian Evolution of the North China Craton. Elsevier, pp. 1–194.

Zheng, J.P., Griffin, W.L.O., Reilly, S.Y., 2004. 3.6 Ga lower crust in central China: new evidence on the assembly of the North China Craton. Geology 32, 229–232.

Zhu, G., Xu, J.W., Sun, S.Q., 1995. Isotopic age evidence for the timing of strike-slip movement of the Tan–Lu Fault zone. Geol. Rev. 41, 452–456 (in Chinese with English abstract).

Zhu, G., Liu, G.S., Song, C.Z., Wang, D.X., 2000. Pulsative extensional activities of the Tan–Lu Fault zone. Geol. J. China Univ. 6, 396–404 (in Chinese with English abstract).

Zhu, G., Wang, D.X., Liu, G.S., Song, C.Z., Xu, J.W., Niu, M.L., 2001. Extensional activities along the Tan–Lu Fault zone and its geodynamic setting. Chin. J. Geol. 36, 269–278 (in Chinese with English abstract).

Zhu, G., Xie, C.L., Wang, Y.S., Niu, M.L., Liu, G.S., 2005. Characteristics of the Tan–Lu high-pressure strike-slip ductile shear zone and its $^{40}Ar/^{39}Ar$ dating. Acta Petrol. Sin. 21, 1687–1702 (in Chinese with English abstract).

Zhu, G., Niu, M.L., Xie, C.L., Wang, Y.S., 2010. Sinistral to normal faulting along the TanLu Fault Zone: evidence for geodynamic switching of the East China Continental Margin. J. Geol. 118 (27), 7–293.